

Studies on 3D domain swapping of azurin from
Alcaligenes xylosoxidans

アルカリジェネシスキシロソキシダンス由来アズリンの
3D ドメインスワッピングに関する研究

ACADEMIC DISSERTATION

ROBBY NOOR CAHYONO

2020 March

Graduate School of Materials Science

Nara Institute of Science and Technology

Supramolecular Science

Contents

Chapter 1	General introduction	1
1.1	Protein oligomerization	2
1.2	Domain swapping	4
1.3	Copper proteins	7
1.4	Azurin	10
1.5	Purpose of this study	15
	References	16
Chapter 2	Oligomerization of azurin	22
2.1	Introduction	23
2.2	Material and methods	24
2.2.1	Azurin-I from <i>Alcaligenes xylosoxidans</i> GIFU1051	24
2.2.2	<i>E. coli</i> culture and azurin purification.	24
2.2.3	Azurin oligomerization.....	26
2.2.4	Dimer purification.	27
2.2.5	Dimer characterization.	28
2.3	Results	30
2.3.1	Azurin purification	30
2.3.2	Azurin oligomerization.....	31
2.3.3	Dimer purification	37
2.3.3	Spectroscopic and electrochemical characterization of azurin dimer	40
2.4	Discussion.....	46
2.5	Conclusion.....	47

References	48
Chapter 3 X-ray crystal structure of azurin dimer	51
3.1 Introduction	52
3.2 Materials and methods.....	54
3.2.1 X-ray crystallographic analysis.....	54
3.3 Results	56
3.3.1 Protein structure.....	56
3.3.2 Active site structure	62
3.4 Discussion.....	65
3.5 Conclusion.....	68
References	69
Chapter 4 General conclusion	74
Acknowledgment.....	77
List of Publication	79

Chapter 1

General introduction

1.1. Protein oligomerization

Protein oligomers have gained interest, owing to their increased knowledge in cells and promising utilization for future materials. Proteins are ‘biologically functional molecules’ that are involved in all fundamental processes in life. Proteins have evolved to be part of the sophisticated and highly efficient molecular machinery that controls the function of the cell, such as transcription, catalysis, metabolism, transport, and structural integrity [1]. Concomitantly, interest in protein–protein interactions has grown in the drug development and chemical biology fields [2], because protein–protein interactions are key factors to consider for conventional drug targets, such as enzymes and transcription factors [3]. Hydrophobic and electrostatic interactions play significant roles in protein–protein interactions, where shape complementarity and chemical components may implement selectivity [4].

Oligomeric proteins, comprising two or more polypeptide chains, represent a significant fraction of proteins in cells. The broad category of oligomeric proteins can be classified by the subunit type, strength of subunit association, and duration and avidity of subunit association [5]. Inter-subunit interfaces share common features containing hydrophobic cores and/or polar surfaces [5]. Functional control, such as allosteric regulation and the establishment of higher-order complexity, may be advantageous features for oligomeric proteins from the perspective of protein evolution. Protein oligomerization has probably evolved by a variety of mechanisms. Many primitive proteins are homo- or hetero-oligomeric to effectively function; thus, the study of the nature of protein oligomerization may elucidate features of protein evolution.

A recent survey suggests that 35% or more of the proteins in a cell are oligomeric [6]. The proportion of oligomeric protein structures deposited in the Protein Data Bank is significantly lower [7]. However, this may simply reflect experimental constraints favoring the structural determination of small monomeric proteins. Most of the oligomeric proteins are homo-oligomers [6]. Higher-order oligomers are less prevalent [6, 7], and a relatively small fraction of oligomeric structures have odd-numbered stoichiometry. Essentially all homo-oligomeric proteins are symmetrical. The most frequently symmetric is cyclic, dihedral, or cubic [6].

The association between subunits can vary in strength and duration. Some proteins are found only, or primarily, in an oligomeric state [5], whereas other proteins have a weak tendency to associate depending on environmental conditions, such as concentration, temperature, and pH. Some proteins may oligomerize dynamically in response to a stimulus, such as nucleotide binding, nucleotide hydrolysis, and phosphorylation state [8].

A homo-dimeric protein has an isologous inter-subunit interaction between the same surfaces of two subunits, giving rise to a dimer with 2-fold symmetry. A heterologous interaction, with two complementary sites, is possible for higher oligomers [5, 9]. Such an interaction can give rise to a discrete oligomer if the interaction is circularly symmetrical or can lead to indefinite self-association if it is not, as in the case of actin [9]. These classifications provide a valuable framework for thinking about protein interfaces, but may not adequately encompass domain swapping [6].

1.2. Domain swapping

Three-dimensional (3D) domain swapping is the process by which two identical proteins exchange the identical structural element ("domain") of their structures to form an intertwined dimer or high-order oligomers. This phenomenon has been observed in many proteins. If both the monomer and the dimer of a molecule exist in stable forms, in which the dimer adopts a domain-swapped conformation and the monomer adopts a closed conformation, the protein is considered to be a bona fide example of 3D domain swapping [10] (Figure 1.1).

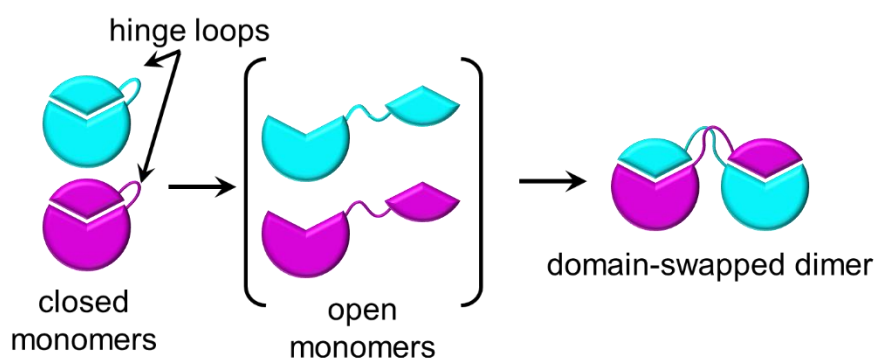


Figure 1.1 Schematic diagram illustrating terms related to 3D domain swapping.

The concept of 3D domain swapping can be traced back about 60 years ago. Bovine pancreatic ribonuclease (RNase A) forms dimers during lyophilization in acetic acid. Based on elegant chemical modification experiments, Crestfield and co-workers proposed in 1962 that a dimer of RNase A forms by exchanging the N-terminal fragments [11]. The term '3D domain swapping' was first used to describe the structure of a diphtheria toxin dimer [12] (Figure 1.2). This mechanism is essentially identical to what is now called 3D domain swapping. The swapped domain can be as large as an entire

globular domain or can be as small as an α -helix or a β -strand. The swapped domains can be either the N terminus or the C terminus, or both of those.

Since the report of the diphtheria toxin dimer, the domain swapping phenomenon has been observed in many proteins [10], including heme proteins such as cytochrome (cyt) *c* [13], cyt *cb*₅₆₂ [14], cyt *c'* [15], and myoglobin [16] (Figure 1.2). Recently, domain swapping has also been used to construct self-assembling artificial nanoarchitectures [14, 17–19] and control protein functions [20, 21].

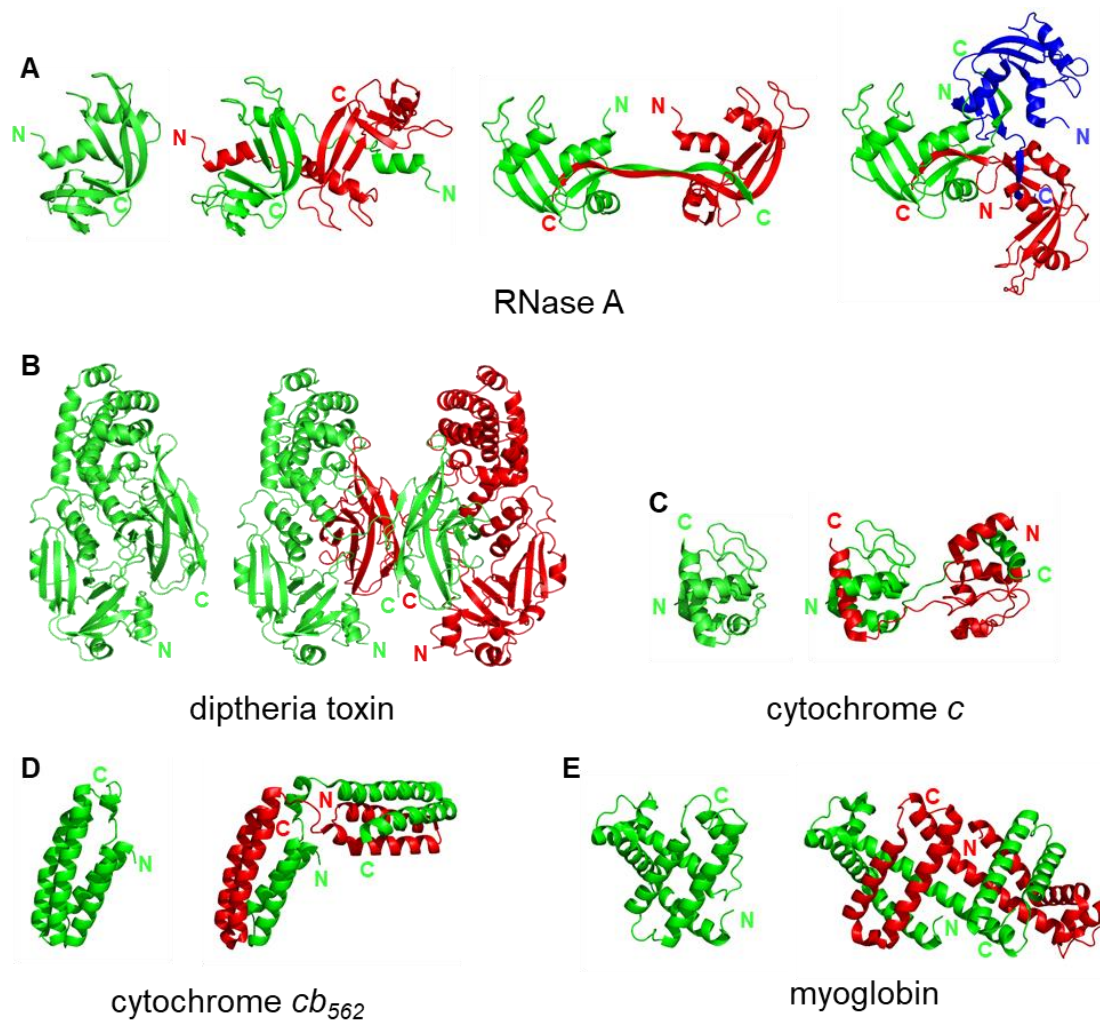


Figure 1.2 Proteins that form oligomers by domain swapping: Crystal structures of (A) RNase A monomer (PDB ID: 5RSA), N-terminal domain-swapped dimer (PDB ID: 1A2W), C-terminal domain-swapped dimer (PDB ID: 1F0V) and trimer (PDB ID: 1JS0); (B) diphtheria toxin monomer (PDB ID: 1MDT) and domain-swapped dimer (PDB ID: 1DDT); (C) cytochrome *c* monomer (PDB ID: 1HRC) and domain-swapped dimer (PDB ID: 3NBS); (D) cytochrome *cb*₅₆₂ monomer (PDB ID: 3HNK) and domain-swapped dimer (PDB ID: 5AWI); and (E) myoglobin monomer (PDB ID: 1MBN) and domain-swapped dimer (3VM9).

1.3. Copper proteins

Copper is the second most abundant transition metal ion in nature after iron [22]. Like iron, copper is a redox-active metal and although essential, it is potentially toxic. To avoid toxicity and overcome solubility problems of Cu(I), the intracellular concentration of Cu is regulated via dedicated proteins that facilitate its uptake and efflux as well as distribution to target Cu-dependent proteins and enzymes [23]. In living systems, copper exists in two stable redox forms: Cu(I) and Cu(II). Like most metals that play roles in living cells, copper carries out various physiological functions in association with specific proteins. Proteins that contain one or more coppers are called ‘copper proteins’. The copper center in a copper protein has been traditionally classified into three types based on their spectroscopic features [24], particularly by electronic absorption and electron paramagnetic resonance spectra [25].

Type 1 copper proteins are characterized by a single copper atom center typically coordinated with histidine, cysteine, and methionine in a distorted tetrahedral structure [25] (Figure 1.3 A). Type 1 copper proteins are also characterized by an extraordinarily intense absorption band near 600 nm, a relatively high redox potential, and an unusually small hyperfine coupling constant for the paramagnetic [oxidized Cu(II)] form of the protein [26]. Type 1 copper proteins are usually called as ‘cupredoxins’ that refer to a group of copper proteins that share the same structural fold and perform biological electron transfer through their redox reactivities [26, 27]. The term cupredoxin comes from ‘ferredoxin’, the Fe-containing redox protein [25]. Examples for this type of copper proteins are azurin, plastocyanin, stellacyanin, nitrite reductase, and laccase [25–27].

Type 2 copper proteins are characterized by a single copper atom center typically coordinated with histidine, aspartic acid, and tyrosine in a distorted tetragonal structure [25] (Figure 1.3 B). Type 2 copper proteins have a weak absorption band at ~700 nm and a larger hyperfine coupling constant, and are paramagnetic in the Cu(II) form [26]. Type 2 copper proteins are found in enzymes that function as catalysts [28]. The examples of this group are superoxide dismutase, galactose oxidase, amine oxidase, nitrite reductase, and laccase [25].

Type 3 copper proteins consist of a pair of coppers, each copper coordinated with three histidine residues in a trigonal planar geometry [27] (Figure 1.3 C). It is characterized by a strong absorption at ~330 nm and an antiferromagnetic feature [26]. Type 3 copper protein are found in catalysis and oxygen transport proteins [27]. Hemocyanin, tyrosinase, and catechol oxidase are included in this group [25].

Recently, two new copper centers that do not belong to the three traditional types of copper centers have been discovered and characterized: Cu_A [29] and Cu_Z [30]. The Cu_A center proteins are characterized by two copper atoms that are coordinated by two histidine, one methionine, a protein backbone carbonyl oxygen, and two bridging cysteine residues [31] (Figure 1.3 D). It is also characterized by strong absorption bands at 480 and 530 nm [25, 27]. This type of protein is also involved in electron transfer. Cyt *c* oxidase, N_2O reductase and menaquinol are members of this group of proteins. The Cu_Z center proteins consist of four copper atoms that are coordinated by seven histidines and bridged by sulfur atoms [25] (Figure 1.3 E). It is characterized by a strong absorption at ~640 nm. N_2O reductase is an example of this group of proteins.

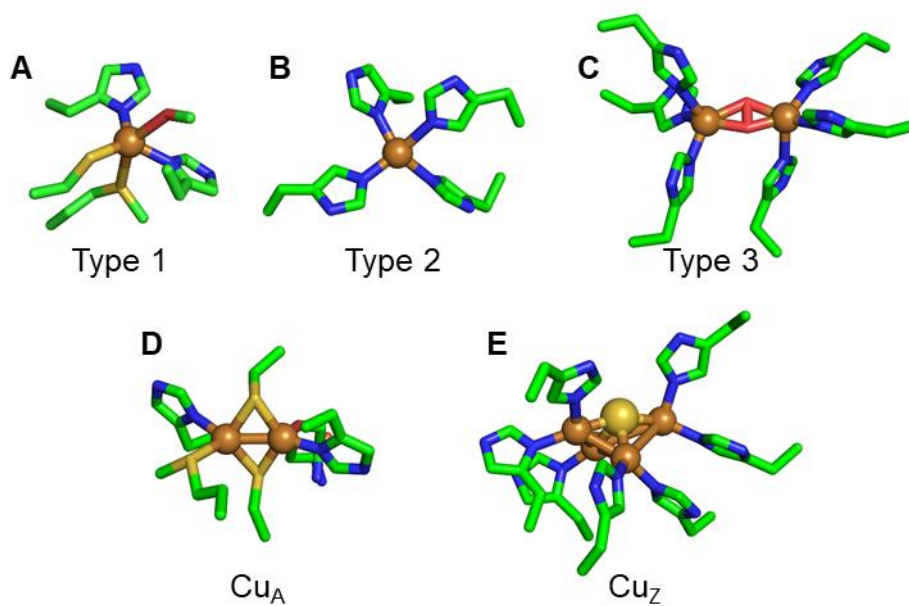


Figure 1.3 Copper centers in copper proteins. (A) Azurin (PDB ID: 1RKR). (B) Superoxide dismutase (PDB ID: 2SOD). (C) Hemocyanin (PDB ID: 1NOL). (D) Cytochrome *ba*₃ (PDB ID: 2CUA). (E) N₂O reductase (PDB ID: 1FWX).

1.4. Azurin

Azurin is a small (~14 kDa) blue-copper protein (belonging to the cupredoxin family) that is believed to facilitate electron transfer in denitrification/respiration chains [26]. Its redox partners, cytochrome *c*₅₅₁ and nitrite reductase, have been identified from *in vitro* experiments, but their relevance as physiological partners has not been established *in vivo* [32]. It has been proposed that the physiological function of azurin in *Pseudomonas aeruginosa* involves electron transfer, directly related to the cellular response to oxidative stress [32]. Azurin has one α -helix and eight β -strands that fold into a β -barrel structure arranged in a double-wound Greek key topology [26, 33] (Figure 1.4). Proteins with the β -barrel motif belong to the large family of sandwich-like proteins. The structures of these proteins are characterized by two β -sheets packed against each other like a sandwich. It was shown that 94% of all sandwich-like proteins contain an invariant substructure consisting of two interlocked pairs of neighboring β -strands with eight hydrophobic positions conserved [34]. In azurin, the two interlocked pairs correspond to β -strands 3 and 4 and β -strands 6 and 7. One may speculate that the minimal transition state for the folding of azurin involves interactions between conserved hydrophobic amino acid residues: Val31, Leu33, Leu50, Tre52, Val95, Phe97, Tyr108, Phe110 [35].

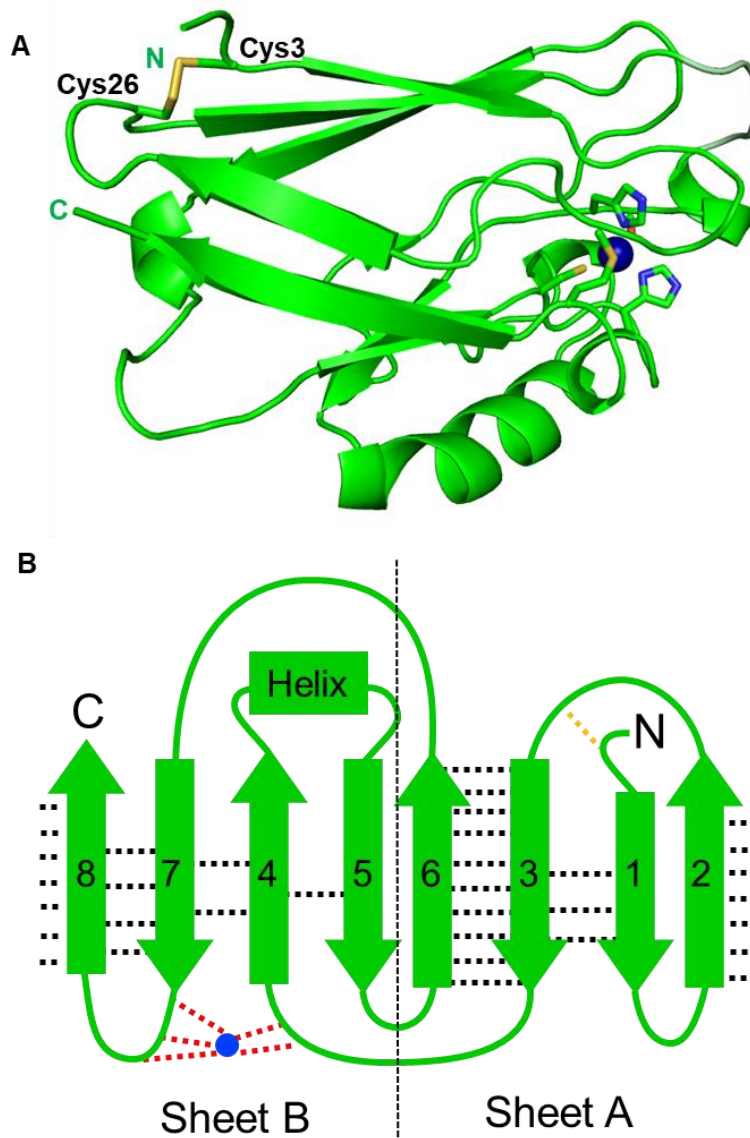


Figure 1.4 (A) Structure of azurin-I from *Alcaligenes xylosoxidans* (PDB ID:1RKR). The disulfide bonds between Cys3 and Cys26 are depicted in yellow. The nitrogen atoms of the side chains of His46 and His117 are depicted in blue, and the sulfur atoms of Cys3, Cys26, Cys112, and Met121 are depicted in yellow. (B) Two-dimensional view of azurin's secondary structure elements. The β strands are represented by arrows, and the α -helix is represented by an elongated box. The two sheets forming the sandwich are indicated and labeled as Sheet A and Sheet B.

Single-molecule force spectroscopy experiments revealed two-state and three-state unfolding pathways for apoazurin and an additional four-state pathway for holoazurin [36]. Steered molecular dynamics (SMD) simulations showed that apoazurin unfold *via* a first transition state (TS), where $\beta 2$ - $\beta 8$ and $\beta 7$ - $\beta 8$ strand pairs rupture to form an intermediate, which subsequently unfolds by the collective rupture of the remaining strands. SMD simulation revealed details of the copper sequestration and predicted a combined $\beta 4$ - $\beta 7$ pair and copper coordination rupture to create the third TS in the four-state pathway [36].

A disulfide bond in the N-terminal region between Cys3 and Cys26 stabilizes the tertiary structure of azurin [37]. The protein structure of azurin defines the geometry of the copper site, leading to an unusual Cu(II) coordination, as in other blue copper proteins [38]. In azurin, two histidine imidazoles (His46 and His117), one cysteine thiolate (Cys112), and two weaker axial ligands—the sulfur atom of methionine (Met121) and the main chain carbonyl oxygen atom of glycine (Gly45)—are coordinated to the copper (Cu(I)/Cu(II)) in a trigonal bipyramidal geometry (Figure 1.5). The active site is located on the edge of the β -barrel, and the residues involved in the metal binding in the unfolded state (Met121, Cys112 and His117) are all in the loop between β -strands 7 and 8 [35]. Beedle and co-workers [39] reported complex unfolding features comprising two-state and three-state pathways in azurin and plastocyanin. The three-state pathway was stochastic, where the unraveling of the protein occurred from either termini. The reaction of the intermediate in the three-state pathway has been attributed to the breaking of Cu-S_{cys} and Cu-N_{his} bonds.

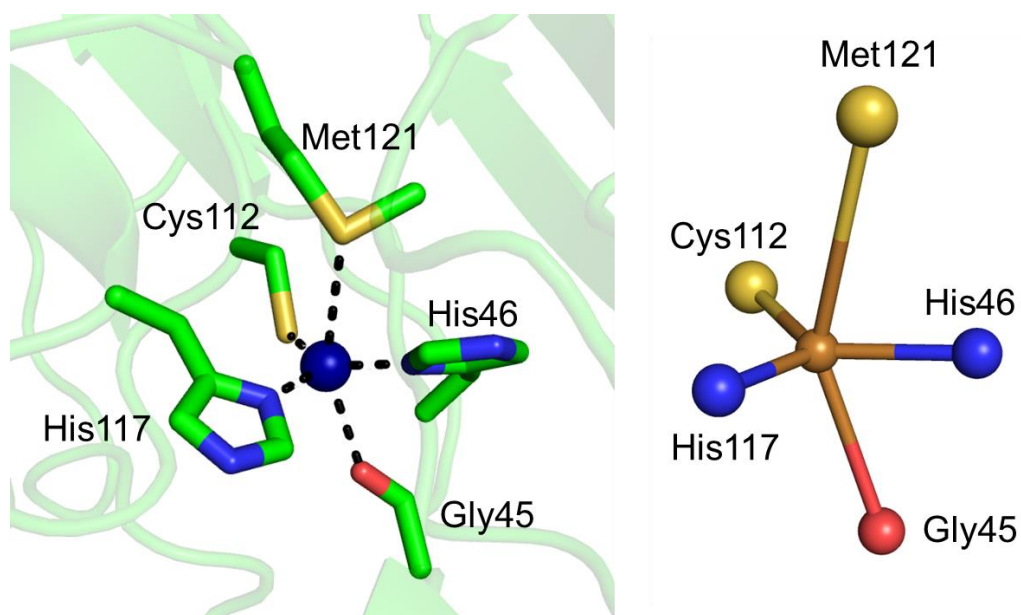


Figure 1.5 Active site structure of azurin. Cu is coordinated by two histidine imidazoles (His117 and His46), one cysteine thiolate (Cys112), and two weaker axial ligands—the sulfur of a methionine (Met121) and the main chain carbonyl oxygen atom of a glycine (Gly45).

Azurins have been models for protein folding and metal binding studies [40, 41]. The 3D structures of azurin with and without a copper ion in the active site are identical, indicating that the copper ion is not mandatory for obtaining a folded structure, although the copper insertion may stabilize the 3D structure [42]. From equilibrium-unfolding experiments of Cu(I)- and Cu(II)-azurins, two-state like transitions were observed for both copper oxidation states, but Cu(II)-azurin was more stable than Cu(I)-azurin [43]. The copper remained bound to the polypeptide of azurin after unfolding, where the copper reduction potential of unfolded azurin was 130 mV higher than that of folded azurin [43]. The higher copper reduction potential of unfolded azurin was achieved by the trigonal Cu(I)-coordination [38]. Thermodynamic cycles connecting the folded apo without copper, unfolded apo with copper, and folded holo, demonstrated that the copper ion

stabilizes the folded form substantially [41]. Folded Cu(I)- and Cu(II)-azurins exhibit folding free energies of -40 and -52 kJ/mol, respectively [43].

Two extreme scenarios have been investigated to address possible pathways for the formation of active azurin (holoazurin): Cu binding before polypeptide folding (path 1) and copper binding after polypeptide folding (path 2) (Figure 1.6). The folding and unfolding kinetics for apoazurin follows a two-state behavior [35, 44, 45]. The extrapolated folding time in water is fast, whereas Cu uptake by folded apoazurin is slow [44, 45]. In contrast, the formation of holoazurin is much faster when the polypeptide folds in the presence of Cu [44, 46]. Holoazurin formation follows path 1, with rapid Cu uptake before polypeptide folding. Thus, introducing Cu prior to protein folding results in more than 1000-fold faster formation of holoazurin [44, 45]. Thus, if time of biosynthesis should be minimized in the cell, Cu coordination before folding is the best approach.

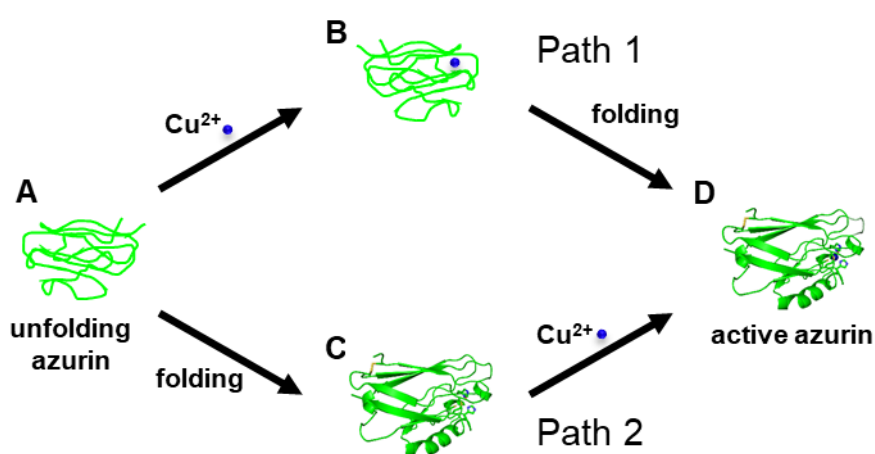


Figure 1.6 The two extreme paths to form active holoazurin: path 1, copper binding to the unfolded protein followed by polypeptide folding (A-B-D); path 2, polypeptide folding, followed by copper binding to the folded apo protein (A-C-D).

1.5. Purpose of this study

Although the properties of blue copper proteins have been elucidated in details, until now, there has been no report on domain swapping of a blue copper protein. In this study, to investigate whether domain swapped oligomerization occurs in copper proteins, the oligomerization condition was searched for *Alcaligenes xylosoxidans* azurin-I, one of the two azurins isolated from *Alcaligenes xylosoxidans* GIFU 1051. Azurin oligomers were obtained, and the azurin dimer was characterized by heat stability, absorption spectroscopy, circular dichroism spectroscopy, electron paramagnetic resonance spectroscopy, cyclic voltammetry, and x-ray crystallography.

References

- [1] Petsko, G.A., Ringe, D., Protein structure and function. New Science Press, 2004.
- [2] Bonetta, L., Interactome under construction. *Nature* 2010, *468*, 851–854.
- [3] Milroy, L.G., Grossmann, T.N., Hennig, S., Brunsveld, L., et al., Modulators of protein-protein interactions. *Chem. Rev.* 2014, *114*, 4695–4748.
- [4] Keskin, O., Gursoy, A., Ma, B., Nussinov, R., Principles of protein–protein interactions: what are the preferred ways for proteins to interact? *Chem. Rev.* 2008, *108*, 1225–1244.
- [5] Ali, M.H., Imperiali, B., Protein oligomerization: How and why. *Bioorganic Med. Chem.* 2005, *13*, 5013–5020.
- [6] Goodsell, D.S., Olson, A.J., Structural symmetry and protein function. *Annu. Rev. Biophys. Biomol. Struct.* 2000, *29*, 105–153.
- [7] Jones, S., Thornton, J.M., Review Principles of protein-protein interactions. *Proc. Natl. Acad. Sci. U. S. A.* 1996, *93*, 13–20.
- [8] Nooren, I.M.A., Thornton, J.M., Structural characterisation and functional significance of transient protein-protein interactions. *J. Mol. Biol.* 2003, *325*, 991–1018.
- [9] Monod, J., Wyman, J., Biol, J.C., On the nature of allosteric transitions: a plausible model. *J. Mol. Biol.* 1965, 88–118.
- [10] Liu, Y., Eisenberg, D., 3D domain swapping: as domains continue to swap. *Protein Sci.* 2002, *11*, 1285–1299.
- [11] Crestfield, A.M., Stein, W.H., Moore, S., On the preparation of bovine pancreatic ribonuclease A. *J. Biol. Chem.* 1963, *238*, 618–621.

- [12] Bennett, M.J., Choe, S., Eisenberg, D., Domain swapping: entangling alliances between proteins. *Proc. Natl. Acad. Sci.* 1994, *91*, 3127–3131.
- [13] Hirota, S., Hattori, Y., Nagao, S., Taketa, M., et al., Cytochrome *c* polymerization by successive domain swapping at the C-terminal helix. *Proc. Natl. Acad. Sci.* 2010, *107*, 12854–12859.
- [14] Miyamoto, T., Kuribayashi, M., Nagao, S., Shomura, Y., et al., Domain-swapped cytochrome *cb*₅₆₂ dimer and its nanocage encapsulating a Zn-SO₄ cluster in the internal cavity. *Chem. Sci.* 2015, *6*, 7336–7342.
- [15] Yamanaka, M., Hoshizumi, M., Nagao, S., Nakayama, R., et al., Formation and carbon monoxide-dependent dissociation of *Allochromatium vinosum* cytochrome *c'* oligomers using domain-swapped dimers. *Protein Sci.* 2017, *26*, 464–474.
- [16] Nagao, S., Osuka, H., Yamada, T., Uni, T., et al., Structural and oxygen binding properties of dimeric horse myoglobin. *Dalt. Trans.* 2012, *41*, 11378–11385.
- [17] Lin, Y.W., Nagao, S., Zhang, M., Shomura, Y., et al., Rational design of heterodimeric protein using domain swapping for myoglobin. *Angew. Chem. Int. Ed. Engl.* 2015, *54*, 511–515.
- [18] Kobayashi, N., Yanase, K., Sato, T., Unzai, S., et al., Self-assembling nano-architectures created from a protein nano-building block using an intermolecularly folded dimeric *de novo* protein. *J. Am. Chem. Soc.* 2015, *137*, 11285–11293.
- [19] Oda, A., Nagao, S., Yamanaka, M., Ueda, I., et al., Construction of a triangle-shaped trimer and a tetrahedron using an α -helix-inserted circular permutant of cytochrome *c*₅₅₅. *Chem. - An Asian J.* 2018, *13*, 964–967.

- [20] Reis, J.M., Burns, D.C., Woolley, G.A., Optical control of protein-protein interactions via blue light-induced domain swapping. *Biochemistry* 2014, 53, 5008–5016.
- [21] Karchin, J.M., Ha, J.H., Namitz, K.E., Cosgrove, M.S., et al., Small molecule-induced domain swapping as a mechanism for controlling protein function and assembly. *Sci. Rep.* 2017, 7, 44388 (12 pages).
- [22] Fraústo da Silva, J.J.R., Williams, R.J.P., The biological chemistry of the elements: the inorganic chemistry of life, Oxford University Press, Oxford 2001.
- [23] Robinson, N.J., Winge, D.R., Copper metallochaperones. *Annu. Rev. Biochem.* 2010, 79, 537–562.
- [24] Malkin, R., Malmström, B.G., The state and function of copper in biological systems, in: *Advances in Enzymology and Related Areas of Molecular Biology*, John Wiley & Sons, Inc., 1970, pp. 177–244.
- [25] Lu, Y., Electron transfer: cupredoxins, in: McCleverty, J.A., Meyer, T.J. (Eds.), *Comprehensive Coordination Chemistry II*, Elsevier Science, Oxford 2003, pp. 91–122.
- [26] Adman, E.T., Copper protein structures. *Adv. Protein Chem.* 1991, 42, 145–197.
- [27] Vila, A.J., Fernández, C.O., Copper in electron transfer proteins, in: Bertini, I., Sigel, A., Sigel, H. (Eds.), *Handbook on Metalloproteins*, Marcel Dekker, New York 2001, pp. 813–856.
- [28] Klinman, J.P., Mechanisms whereby mononuclear copper proteins functionalize organic substrates. *Chem. Rev.* 1996, 96, 2541–2561.

- [29] Iwata, S., Ostermeier, C., Ludwig, B., Michel, H., Structure at 2.8 Å resolution of cytochrome *c* oxidase from *Paracoccus denitrificans*. *Nature* 1995, 376, 660–669.
- [30] Brown, K., Tegoni, M., Prudêncio, M., Pereira, A.S., et al., A novel type of catalytic copper cluster in nitrous oxide reductase. *Nat. Struct. Biol.* 2000, 7, 191–195.
- [31] Solomon, E.I., Sundaram, U.M., Machonkin, T.E., Multicopper oxidases and oxygenases. *Chem. Rev.* 1996, 96, 2563–2606.
- [32] Vijgenboom, E., Busch, J.E., Canters, G.W., *In vivo* studies disprove an obligatory role of azurin in denitrification in *Pseudomonas aeruginosa* and show that *azu* expression is under control of RpoS and ANR. *Microbiology* 1997, 143, 2853–2863.
- [33] Mayes, E., Bewick, A., Gleeson, D., Hoinville, J., et al., Biologically derived nanomagnets in self-organized patterned media. *IEEE Trans. Magn.* 2003, 39, 624–627.
- [34] Kister, A.E., Finkelstein, A. V., Gelfand, I.M., Common features in structures and sequences of sandwich-like proteins. *Proc. Natl. Acad. Sci. U. S. A.* 2002, 99, 14137–14141.
- [35] Pozdnyakova, I., Wittung-Stafshede, P., Approaching the speed limit for Greek Key β -barrel formation: transition-state movement tunes folding rate of zinc-substituted azurin. *Biochim. Biophys. Acta* 2003, 1651, 1–4.
- [36] Yadav, A., Paul, S., Venkatramani, R., Ainaravapu, S.R.K., Differences in the mechanical unfolding pathways of apo- and copper-bound azurins. *Sci. Rep.* 2018, 8, 1989 (13 pages).

- [37] Bonander, N., Karlsson, B.G., Vänngård, T., Disruption of the disulfide bridge in azurin from *Pseudomonas aeruginosa*. *Biochim. Biophys. Acta* 1995, 1251, 48–54.
- [38] Wittung-Stafshede, P., Hill, M.G., Gomez, E., Di Bilio, A.J., et al., Reduction potentials of blue and purple copper proteins in their unfolded states: a closer look at rack-induced coordination. *J. Biol. Inorg. Chem.* 1998, 3, 367–370.
- [39] Beedle, A.E.M., Lezamiz, A., Stirnemann, G., Garcia-Manyes, S., The mechanochemistry of copper reports on the directionality of unfolding in model cupredoxin proteins. *Nat. Commun.* 2015, 6, 7894 (9 pages).
- [40] Pozdnyakova, I., Wittung-Stafshede, P., Stability and folding of copper-binding proteins, in: Gomes, C.M., Wittung-Stafshede, P. (Eds.), *Protein Folding and Metal Ions*, CRC Press, Boca Raton 2010, pp. 61–80.
- [41] Ariöz, C., Wittung-Stafshede, P., Folding of copper proteins: role of the metal? *Q. Rev. Biophys.* 2018, 51, 1–39.
- [42] Nar, H., Messerschmidt, A., Huber, R., van de Kamp, M., et al., Crystal structure of *Pseudomonas aeruginosa* apo-azurin at 1.85 Å resolution. *FEBS Lett.* 1992, 306, 119–124.
- [43] Leckner, J., Wittung, P., Bonander, N., Karlsson, B.G., et al., The effect of redox state on the folding free energy of azurin. *J. Biol. Inorg. Chem.* 1997, 2, 368–371.
- [44] Pozdnyakova, I., Wittung-Stafshede, P., Biological relevance of metal binding before protein folding. *Proc. Natl. Acad. Sci. U.S.A* 2000, 297, 10135–10136.
- [45] Pozdnyakova, I., Wittung-Stafshede, P., Copper binding before polypeptide folding speeds up formation of active (holo) *Pseudomonas aeruginosa* azurin.

Biochemistry 2001, 40, 13728–13733.

- [46] Pozdnyakova, I., Guidry, J., Wittung-Stafshede, P., Copper stabilizes azurin by decreasing the unfolding rate. *Arch. Biochem. Biophys.* 2001, 390, 146–148.

Chapter 2

Oligomerization of azurin

2.1 Introduction

Various *c*-type cytochromes have been shown to domain swap by the procedure of an addition of alcohol, lyophilization, and dissolution in buffer [1–3]. Myoglobin forms a domain-swapped dimer by the treatment with ethanol [4]. Domain-swapped dimer of cytochrome *cb₅₆₂* was obtained by the treatment of its monomer with acetic acid, where two α -helices in the N-terminal region in a protomer interacted with two α -helices in the C-terminal in the other protomer [1]. The treatment of horse ferric cytochrome *c* monomer with ethanol formed domain-swapped oligomers (dimer and trimer) by swapping the C-terminal α -helix [5]. It has been reported that horse cytochrome *c* forms oligomers during protein folding [6, 7], and more domain-swapped oligomers were formed for higher protein concentrations during folding of horse cytochrome *c* [6].

Since there is no report on oligomerization of copper proteins, in this chapter I tried to oligomerize azurin by a similar procedure that was used for the oligomerization of cytochrome *c*. I focused on the purification and characterization of the azurin dimer because the dimer is the simplest oligomer.

2.2 Material and methods

2.2.1 Azurin-I from *Alcaligenes xylosoxidans* GIFU1051

Azurin-I from *Alcaligenes xylosoxidans* GIFU1051 was produced from *E. coli* BL21(DE3) cells containing the pTAZ 1-1 plasmid with the azurin-I gene of *Alcaligenes xylosoxidans* GIFU1051. The amino acid sequence of azurin-I is shown below:

```

      10           20           30           40           50
      |           |           |           |           |
AECSVDIAGN DQMQFDKKEI TVSKSCKQFT VNLKHPGKLA KNVMGHNWVL
      60           70           80           90          100
      |           |           |           |           |
TKQADMQGAV NDGMAAGLDN NYVKKDDARV IAHTKVIGGG ETDSVTFDVS
      110          120          129
      |           |           |
KLAAGQDYAY FCSFPGHFAL MKGVCLKLVD
```

2.2.2 *E. coli* culture and azurin purification

E. coli BL21(DE3) cells containing the pTAZ 1-1 plasmid with the azurin-I gene of *Alcaligenes xylosoxidans* GIFU1051 (obtained from Prof. Kunishige Kataoka, Kanazawa University) were incubated in 10 mL of Luria-Bertani (LB) media containing 100 µg/mL ampicillin at 37 °C for 7–8 h. The culture was transferred into 2 L of LB media containing 100 mg/L ampicillin and 1 mM CuCl₂, and subsequently incubated at 37 °C. When the OD₆₀₀ reached 0.6 after about 3.5 h of culture, isopropyl β-D-1-thiogalactopyranoside (Wako; final conc. 0.5 mM) was added to the culture. After the culture was further incubated under the same conditions for 12 h, the cells were harvested by centrifugation at 8000 rpm and 4 °C for 5 min.

Azurin-I was purified by a previously reported method with modifications.[8] The cultured *E. coli* cell pellet (8 g) was suspended in 160 mL of 30 mM Tris-HCl buffer, pH 8.3, containing 20% sucrose and 1 mM ethylenediaminetetraacetic acid (Wako). The suspension was stirred at room temperature for 15 min, and centrifuged at 5000 g and 4 °C for 15 min. The pellet was quickly resuspended in 250 ml of cold water (4 °C) for osmotic shock, and stirred for 15 min. After centrifugation at 5000 g and 4 °C for 15 min, CuSO₄ (final conc., 1 mM) was added to the supernatant, and the solution was stirred at room temperature for 1 h. Potassium ferricyanide (final conc., 0.1 mM) was further added to the solution, and the solution was stirred at room temperature for 1 h. The pH of the solution was adjusted to 4.0 by an addition of acetic acid. After centrifugation of the pH-adjusted solution at 5000 g and 4 °C for 15 min, the blue supernatant was purified by cation exchange chromatography (carboxymethyl cellulose, TOSOH) using an open column (ϕ2.8 cm × 15 cm) at room temperature with 50 mM ammonium acetate buffer, pH 4.0. The protein was eluted with 50 mM ammonium acetate buffer, pH 4.0, containing 50 mM NaCl. The fractions containing azurin were concentrated and then purified by size exclusion chromatography (SEC; HiLoad 26/60 Superdex 75, GE Healthcare) using a fast protein liquid chromatography (FPLC) system (BioLogic DuoFlow 10, Bio-Rad) with 50 mM sodium acetate buffer, pH 5.0, at 4 °C. Dithiothreitol (DTT)-reduced azurin was prepared by reduction of Cu(II)-azurin with DTT (Nacalai tesque), and removing DDT from the DTT-reduced azurin solution by ultrafiltration (Amicon Ultra-15, Merck Millipore). Cu(I)-azurin was prepared by reduction of Cu(II)-azurin with potassium ferrocyanide, and removing potassium ferrocyanide from the Cu(I)-azurin solution by anion exchange chromatography (diethylaminoethyl cellulose (DEAE), TOSOH) by

passing the solution through an open column ($\phi 1.5 \text{ cm} \times 6.0 \text{ cm}$) at room temperature. Apoazurin was prepared by the method previously reported [9].

2.2.3 Azurin oligomerization

Cu(II)-azurin was oligomerized at pH 4.0–7.0 by treatment with ethanol, 2,2,2-trifluoroethanol (TFE), or 2-mercaptoethanol (2-ME) by the following procedure. The azurin solution was lyophilized after an addition of ethanol (final conc., 70 % (v/v)), TFE, (final conc., 5 % (v/v)) or 2-ME (final conc., 140 mM), and the obtained precipitate was dissolved in 50 mM potassium phosphate buffer, pH 7.0. Subsequently, CuSO_4 (final conc., 5 mM) was added to the azurin solution, and the solution was incubated at room temperature for 1 h. DTT (final conc., 40 mM) was further added to the incubated azurin solution to reduce the disulfide bonds that may form oligomers, and the solution was incubated at room temperature for 3 h. After the solution was centrifuged and filtered to remove precipitates, the solution was analyzed by SEC (Superdex 75 10/300 GL, GE Healthcare) using the FPLC system (BioLogic DuoFlow 10) with 50 mM potassium phosphate buffer, pH 7.0, at 4 °C.

Various conditions were investigated for the oligomerization of Cu(II)-azurin by the treatment with 2-ME at pH 4.0. To investigate the 2-ME concentration dependence on the oligomerization of Cu(II)-azurin, similar procedures using different 2-ME concentrations (final conc. 70, 140, 280, 420, and 560 mM) were performed. Similar procedures using different Cu(II)-azurin concentrations (final conc. 0.5, 1.0, 1.5, 2.0, and 3.0 mM) were performed to investigate the protein concentration dependence on the oligomerization. To investigate the effect of DTT after dissolution of the lyophilized azurin with buffer, DTT was added to the solution with different concentrations (final conc. 0, 10, 20, 30, and 40

mM) after lyophilization, dissolution, addition of CuSO₄ (final conc., 5 mM), and incubation at room temperature for 1 h.

To elucidate the effects of the copper oxidation state and disulfide bond formation on azurin oligomerization, Cu(I)-, Cu(II)-, and DTT-reduced azurins were oligomerized by an addition of TFE (final conc., 5 % (v/v)) with a similar procedure, except at pH 5.0, because Cu(I)-azurin precipitated at pH 4.0. To investigate the effect of Cu(II) ions on the azurin oligomerization at the dissolution (refolding) process, apoazurin was lyophilized at pH 4.0 in the presence of 140 mM 2-ME, followed by dissolution (final conc. of apoazurin, 5 mM) in Tris-HCl buffer, pH 7.4, containing 5 mM CuCl₂ (or CaCl₂) or dissolution in the Tris-HCl buffer not containing CuCl₂ and CaCl₂. CuCl₂ (final conc., 5 mM) was added to the azurin solution 5 min after the lyophilized solution was dissolved in the absence of CuCl₂.

2.2.4 Dimer purification

To obtain the azurin dimer, oligomerization was performed by the addition of 2-ME (final conc., 140 mM) to Cu(II)-azurin (final conc., 1.5 mM) in 50 mM ammonium acetate buffer, pH 4.0. The azurin solution was lyophilized, dissolved in phosphate buffer, pH 7.0, and subsequently CuSO₄ (final conc., 5 mM) was added to the solution. After incubation of the azurin solution at 25 °C for 1 h, DTT (final conc., 40 mM) was added to the solution, and the solution was further incubated at room temperature for 3 h. The solution was centrifuged and filtered to remove precipitates, and subsequently the azurin dimer was purified by SEC (HiLoad 26/60 Superdex 75) using the FPLC system (BioLogic DuoFlow 10) with 50 mM potassium phosphate buffer, pH 7.0, at 4 °C. The azurin dimer was oxidized by an addition of potassium ferricyanide to the dimer solution, and

potassium ferricyanide was removed from the dimer solution by passing the solution through the DEAE open column ($\phi 1.5 \text{ cm} \times 6.0 \text{ cm}$) with 50 mM potassium phosphate buffer, pH 7.0. The obtained dimer was purified by cation exchange chromatography (MonoS, GE Healthcare) using the FPLC system (BioLogic DuoFlow 10) with a sodium sulfate concentration gradient (0–300 mM) and 50 mM sodium acetate buffer, pH 5.0, at 4 °C, and SEC (HiLoad 26/60 Superdex 75) using the FPLC system (BioLogic DuoFlow 10) under the same conditions as stated above for SEC.

2.2.5 Dimer characterization

The heat stability of the azurin dimer was investigated by incubating the dimer in 50 mM potassium phosphate buffer, pH 7.0, at 60 and 70 °C for 1 h, and subsequently analyzing the solution by SEC (Superdex 75 10/300 GL) using the FPLC system (BioLogic DuoFlow 10) with 50 mM potassium phosphate buffer, pH 7.0, at 4 °C. The molar extinction coefficients of the Cu(II)-azurin monomer and dimer were calculated by measuring the absorption spectrum and copper quantity of the same azurin solution. The absorption spectra of the Cu(II)-azurin monomer and dimer in 50 mM potassium phosphate buffer, pH 7.0, were measured with a UV-2450 spectrophotometer (Shimadzu) using a 1 cm path-length quartz cell at 25 °C. The copper quantities of the same solutions were determined with an ICPM-8500 inductively coupled plasma mass spectrometer (Shimadzu) at 25 °C, where azurin was denatured with aqua regia. The EPR spectra of Cu(II)-azurin monomer and dimer in 100 mM 2-(*N*-morpholino)ethanesulfonic acid (MES) buffer, pH 6.5, were measured with a JES-FA100N electron spin resonance spectrometer (JEOL) at 77 K. The microwave frequency was 9.134 GHz, and the microwave power was 0.998 mW. The circular dichroism (CD) spectra of the Cu(II)-

azurin monomer and dimer (5.0 μM , copper unit) in 50 mM potassium phosphate buffer, pH 7.0, were measured with a J-725 CD spectropolarimeter (Jasco) using a 0.1 cm path-length quartz cell at 25 $^{\circ}\text{C}$. CD ellipticity at 222 nm of azurin monomer (5.0 μM , copper unit) in 50 mM potassium phosphate buffer, pH 7.0 was monitored at 25–95 $^{\circ}\text{C}$ with an increase of 1 $^{\circ}\text{C}/\text{min}$ to measure the protein stability. Cyclic voltammetry (CV) responses of Cu(II)-azurin monomer and dimer (200 μM , copper unit) in 100 mM MES buffer, pH 6.5, were measured with an ALS-612DN electrochemical analyzer (BAS Inc.). An Au electrode was used as a working electrode, and Pt wire and Ag/AgCl (3M NaCl) were used as counter and reference electrodes, respectively. The redox potentials were calculated with respect to the normal hydrogen electrode (NHE). Modification of the surface of the Au electrode was performed by the following procedure[10]. The surface of the Au electrode was polished with 0.05 μm alumina water slurry and subsequently rinsed with pure water. To remove residual organic compounds from the electrode surface, the Au electrode was cleaned by electrochemical oxidation/reduction treatment. The Au electrode was dipped in a methanol solution containing 1 mM 4-mercaptopyridine (Wako) for 1 min, and subsequently rinsed with pure water. All the measurements were performed at room temperature and flowing Ar gas for at least 5 min to remove oxygen dissolved in the solution.

2.3 Results

2.3.1 Azurin purification

The final step for the purification of Cu(II)-azurin is size exclusion chromatography (SEC). The SEC elution curve showed a main peak at 214 mL, corresponding to the azurin monomer (Figure 2.1). The absorption spectrum of Cu(II)-azurin exhibited a strong 622 nm absorption band, which is characteristic of type 1 copper proteins (Figure 2.2). The purity of azurin was confirmed by the ratio of the absorbance at 280 nm to that at ~620 nm. The ratio of the absorbance at 280 nm to that at ~620 nm (Abs_{280}/Abs_{622}) for Cu(II)-azurin was 2.22, whereas the Abs_{280}/Abs_{622} of purified Cu(II)-azurin from *Alcaligenes xylosoxidans* is reported to be 2.23[11]. This result indicated a high purity for the purified azurin.

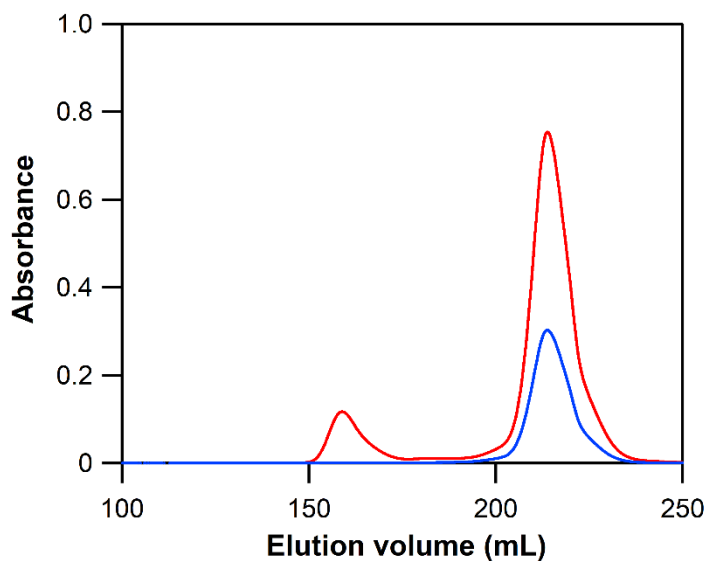


Figure 2.1 SEC chromatograms of Cu(II)-azurin monomer at the final step of purification. Measurement conditions: column, HiLoad 16/600 Superdex 75 column; flow rate, 1.0 mL/min; buffer, 50 mM sodium acetate buffer, pH 5.0; temperature, 4 °C; monitoring wavelength, 280 (red) and 620 nm (blue).

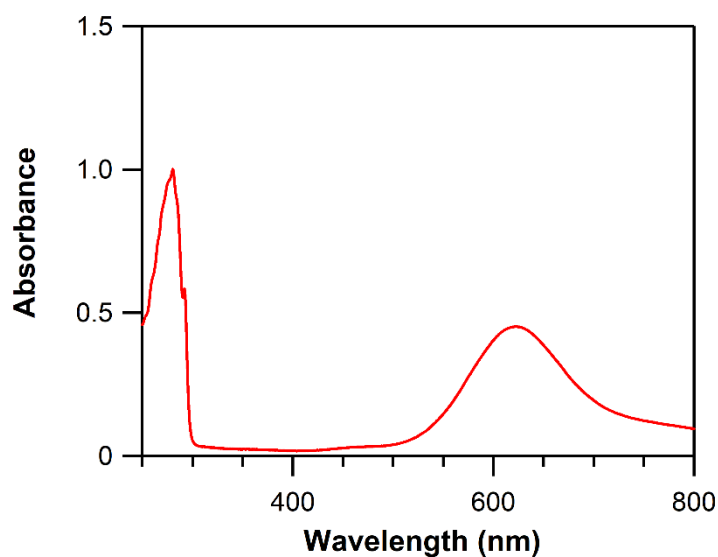


Figure 2.2 Optical absorption spectrum of Cu(II)-azurin in 50 mM potassium phosphate buffer, pH 7.0.

2.3.2 Azurin oligomerization

For azurin-I, only a slight amount of oligomers was obtained by the procedure of an addition of ethanol (final conc., 70 % (v/v)) at pH 4.0 and 7.0 or 2,2,2-trifluoroethanol (TFE) (final conc., 5 % (v/v)) at pH 7.0 to Cu(II)-azurin, lyophilization, and dissolution, whereas a small amount of oligomers was obtained by the same procedure using TFE (final conc., 5 % (v/v)) at pH 4.0 instead of ethanol or TFE (Figure 2.3 A). When performing a similar oligomerization procedure with TFE (final conc., 5 % (v/v)) at pH 5.0 for Cu(I)-azurin, more oligomers were obtained compared to that obtained from Cu(II)-azurin (Figure 2.3 B). Since Cu(I)-azurin is less stable than Cu(II)-azurin [12], Cu(I)-azurin may unfold more easily than Cu(II)-azurin, enhancing the oligomerization process. When DTT-reduced azurin was treated with the oligomerization procedure using TFE (final conc., 5 % (v/v)) at pH 5.0, the amount of high order oligomers increased

(Figure 2.3 B), demonstrating that the disulfide bond inhibits formation of high order oligomers, presumably by steric hindrance. Based on these results, I envisaged that 2-ME may reduce Cu(II) to Cu(I) and the oligomerization procedure using 2-ME for Cu(II)-azurin may show a similar effect as that using TFE for DTT-reduced azurin. The dimer amount increased whereas the higher order oligomer amount decreased when DTT-reduced azurin was treated with 2-ME compare to the corresponding oligomers when Cu(II)-azurin was treated with 2-ME (Figure 2.3 C). These results indicate that formation of higher order oligomers was enhanced by the disulfide bond cleavage.

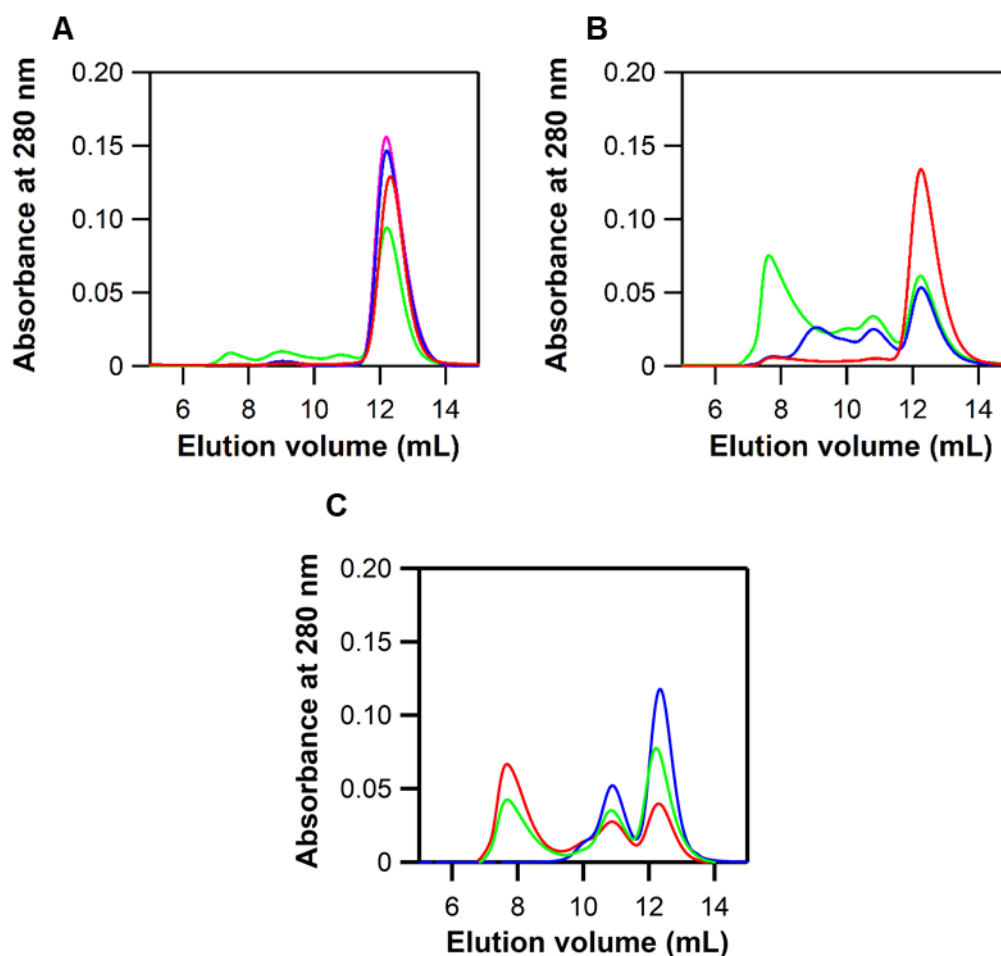


Figure 2.3 SEC chromatograms of azurin after the procedure of an addition of ethanol, TFE, or 2-ME, lyophilization, and dissolution to buffer: (A) Cu(II)-azurin was treated with ethanol (final conc., 70 % (v/v)) at pH 4.0 (red) and pH 7.0 (blue) and TFE (final conc., 5 % (v/v)) at pH 4.0 (green) and pH 7.0 (magenta). (B) Cu(II)- (red), Cu(I)- (blue), and DTT-reduced azurin (green) were treated with TFE (final conc., 5 % (v/v)) at pH 5.0. (C) DTT-reduced azurin (red) was treated with TFE (final conc., 5 % (v/v)) and Cu(II)-azurin (blue) and DTT-reduced azurin (green) were treated with 2-ME (final conc., 140 mM) at pH 4.0. The lyophilized protein was dissolved in 50 mM potassium phosphate buffer, pH 7.0. Measurement conditions: column: Superdex 75 10/300 GL; buffer: 50 mM potassium phosphate buffer, pH 7.0; monitoring wavelength: 280 nm.

Treatment of Cu(II)-azurin with 2-ME at pH 4.0 produced more dimers compared to DTT-reduced azurin treatment with TFE (Figure 2.3 C). To obtain more dimers, I investigated the oligomerization of Cu(II)-azurin with different concentrations of 2-ME. The azurin oligomer amount increased by increasing the concentration of 2-ME (Figure 2.4). Trimers were also detected in the SEC chromatograms by the treatment of Cu(II)-azurin with 2-ME for concentrations higher than 280 mM (Figure 2.4); thus, 140 mM 2-ME was used hereafter.

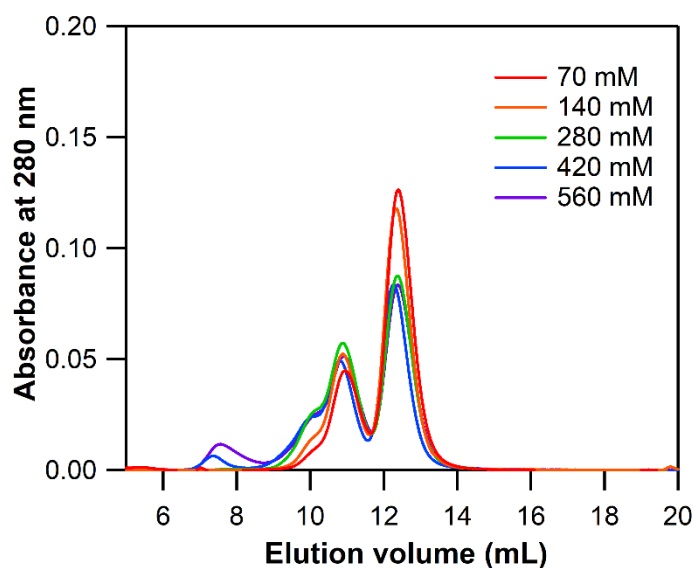


Figure 2.4 SEC chromatograms of azurin after the procedure of addition of 2-ME (final conc. 70, 140, 280, 420, and 560 mM), lyophilization, dissolution with 50 mM potassium phosphate buffer, pH 7.0, addition of 5 mM CuSO₄, and addition of DTT. Measurement conditions: column: Superdex 75 10/300 GL; buffer: 50 mM potassium phosphate buffer, pH 7.0; monitoring wavelength: 280 nm

Protein concentration dependence on Cu(II)-azurin oligomerization by treatment with 2-ME was investigated with various azurin concentrations. The oligomer amount increased by increasing the concentration of azurin (Figure 2.5). The SEC chromatograms

showed that the dimer/monomer ratio was highest for the 1.5 mM azurin among the conditions studied (0.5 mM: 0.55, 1.0 mM: 0.56, 1.5 mM: 0.63, 2.0 mM: 0.59, 3.0 mM: 0.35) (Figure 2.5).

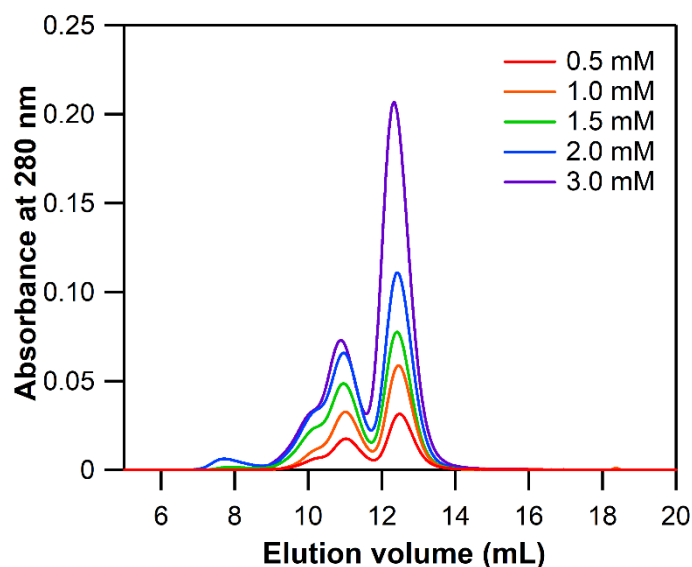


Figure 2.5 SEC chromatograms of azurin (final conc. 0.5, 1.0, 1.5, 2.0, and 3.0 mM) after the procedure of addition of 2-ME, lyophilization, dissolution 50 mM potassium phosphate buffer, pH 7.0, addition 5 mM CuSO_4 , and addition of DTT. Measurement conditions: column: Superdex 75 10/300 GL; buffer: 50 mM potassium phosphate buffer, pH 7.0; monitoring wavelength: 280 nm

The effect of DTT on azurin oligomerization was investigated by an addition of various concentrations of DTT to the oligomer solution after the dissolution of the lyophilized azurin and subsequent addition of 5.0 mM CuSO_4 . The SEC chromatograms showed that higher-order oligomers are detected by the treatment with 30 mM DTT or lower concentration of DTT, but not by the treatment with 40 mM DTT (Figure 2.6). These results indicate that during the oligomerization, oligomers were also formed through intermolecular disulfide (S–S) bonds. Not all intermolecular disulfide bonds were

reduced when DTT was added up to 30 mM, however intermolecular disulfide bonds were reduced after addition of 40 mM DTT.

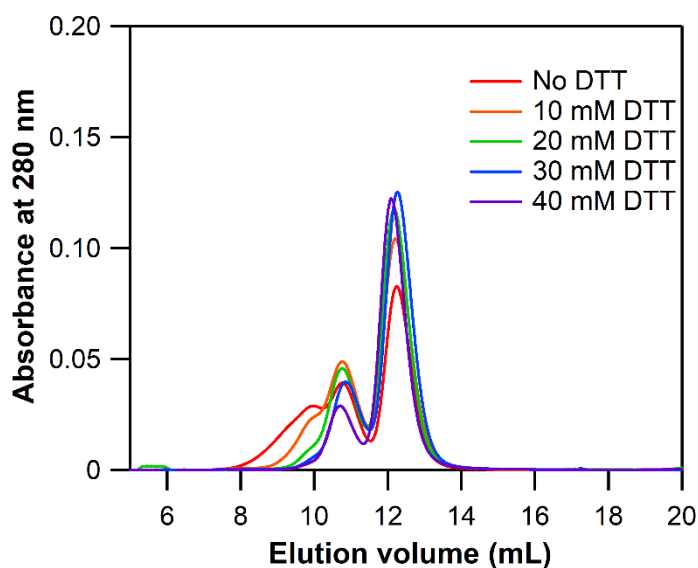


Figure 2.6 SEC chromatograms of azurin after the procedure of addition of 2-ME, lyophilization, dissolution 50 mM potassium phosphate buffer, pH 7.0, addition of 5 mM CuSO_4 , and addition of DTT (final conc. 0, 10, 20, 30, and 40 mM). Measurement conditions: column: Superdex 75 10/300 GL; buffer: 50 mM potassium phosphate buffer, pH 7.0; monitoring wavelength: 280 nm

The effect of Cu(II) ion on azurin oligomerization was investigated by performing a similar procedure using 2-ME with an addition of 5 mM CuCl_2 to the solution of lyophilized apoazurin for dissolution (Figure 2.7). The amount of oligomers increased from 30 % to 51 % by the addition of Cu(II) ions (equal amount to apoazurin) to the solution for dissolution, whereas it did not when 5 mM CaCl_2 was added to the solution for dissolution, indicating that Cu(II) ions enhance oligomerization of azurin.

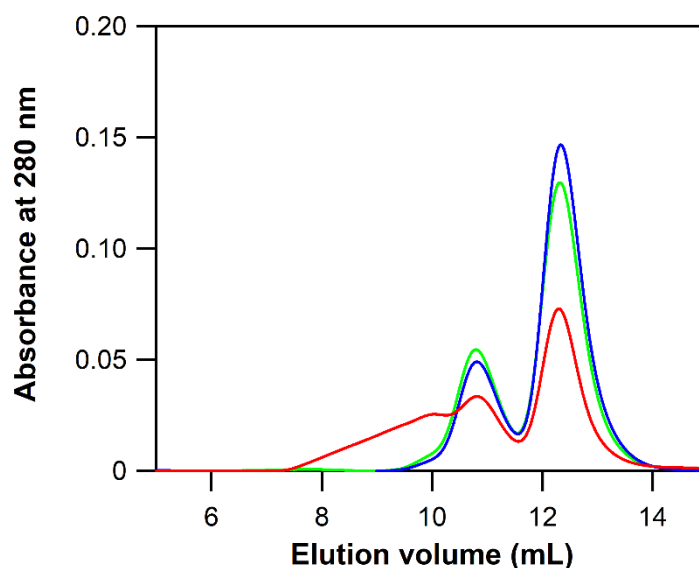


Figure 2.7 SEC chromatograms of azurin after the procedure of an addition of ethanol, TFE, or 2-ME, lyophilization, and dissolution to buffer. Apoazurin was lyophilized at pH 4.0 in the presence of 140 mM 2-ME, followed by dissolution (final conc. of apoazurin, 5 mM) in the buffer containing 5 mM CuCl_2 (red) or CaCl_2 (blue) or the buffer not containing CuCl_2 and CaCl_2 with subsequent addition of CuCl_2 (final conc., 5 mM) (green). The lyophilized protein was dissolved in 50 mM Tris-HCl buffer, pH 7.4. Measurement conditions: column: Superdex 75 10/300 GL; buffer: 50 mM Tris-HCl buffer, pH 7.4; monitoring wavelength: 280 nm.

2.3.3 Dimer purification

Oligomerization of Cu(II)-azurin was performed by the procedure of addition of 2-ME, lyophilization, dissolution, addition of CuSO_4 , and addition of DTT. The DTT-reduced azurin dimer was purified by SEC; fractions at 159–180 mL were collected as solutions containing dimers (Figure 2.8). To oxidize the DTT-reduced azurin dimer in the solution, potassium ferricyanide (final conc., 100 mM) was added to the dimer solution. The absorption spectra of the azurin dimer before and after oxidation with ferricyanide are shown in Figure 2.9. The DTT-reduced azurin dimer was oxidized by ferricyanide and

its absorption spectrum exhibited an absorption band at 618 nm. The absorption at 618 nm increased, indicating that the copper ion in the azurin dimer was oxidized. The Cu(II)-azurin dimer was initially purified by performing ion exchange chromatography (IEC) and collecting the fractions at 26.0–28.5 mL (Figure 2.10). The Cu(II)-azurin dimer was further purified by SEC and collecting the fractions at 159–175 mL (Figure 2.11).

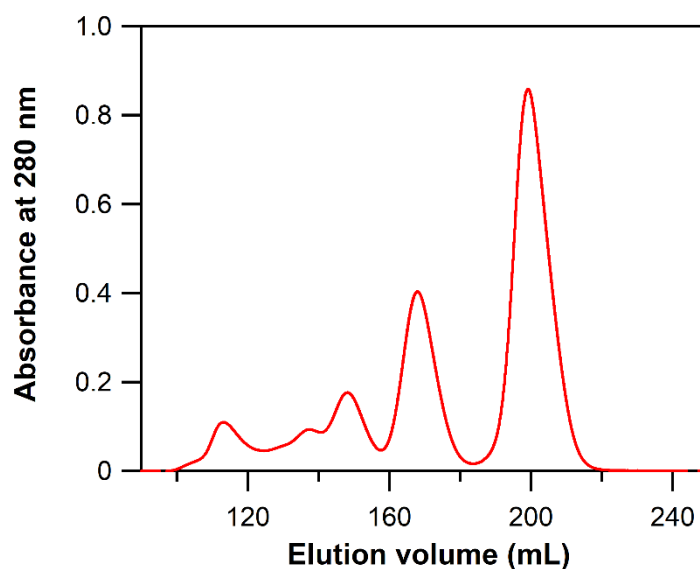


Figure 2.8 SEC chromatogram of DTT-reduce azurin dimer. Measurement conditions: column, HiLoad 16/600 Superdex 75 column; flow rate, 1.0 mL/min; buffer, 50 mM potassium phosphate buffer, pH 7.0; temperature; 4 °C, monitoring wavelength, 280 nm.

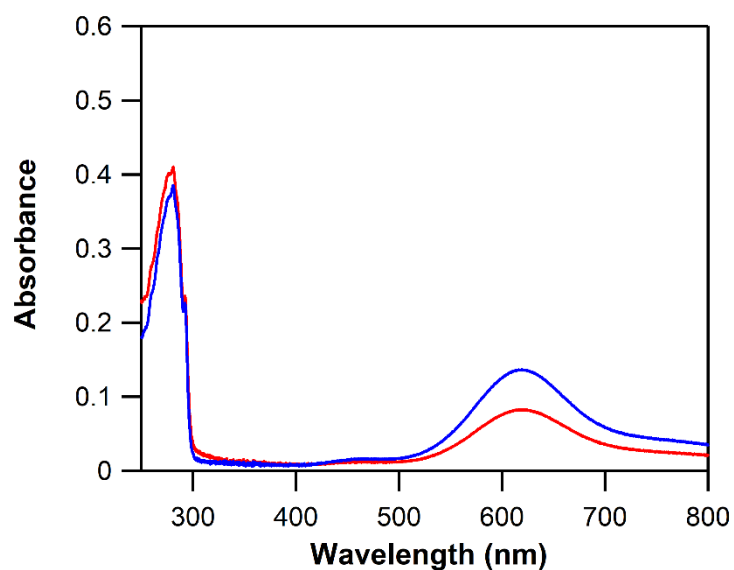


Figure 2.9 Optical absorption spectra of azurin dimer before (red) and after (blue) oxidation with ferricyanide in 50 mM potassium phosphate buffer, pH 7.0.

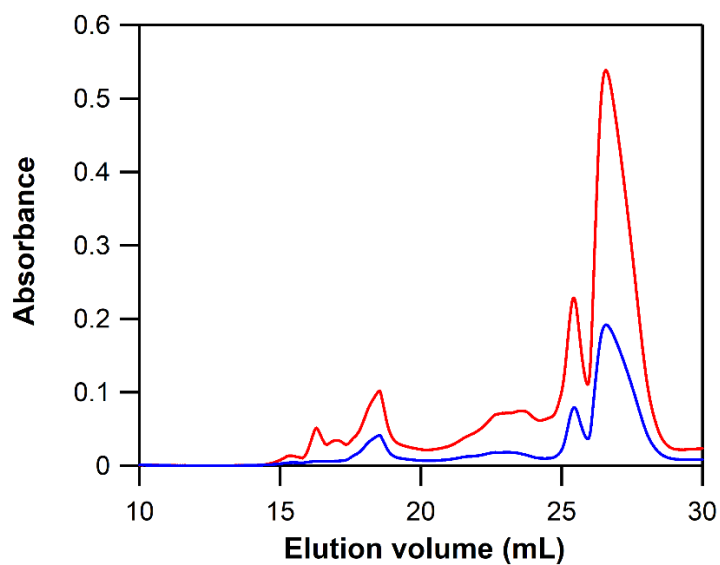


Figure 2.10 IEC chromatograms of Cu(II)-azurin dimer. Measurement conditions: column, MonoS; flow rate, 0.50 mL/min; gradient, 50 mM sodium acetic buffer, pH 5.0, and 50 mM sodium acetic buffer, pH 5.0, containing 300 mM NaSO₄; temperature, 4 °C, monitoring wavelength, 280 (red) and 620 nm (blue).

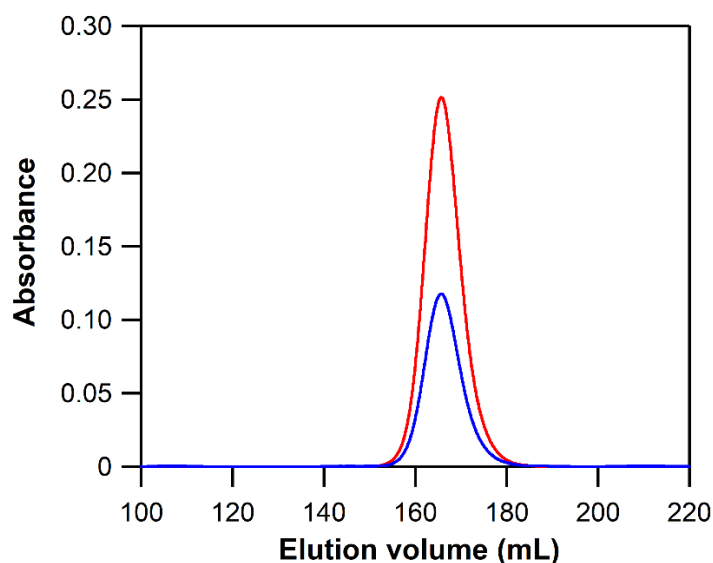


Figure 2.11 SEC chromatograms of Cu(II)-azurin dimer. Measurement conditions: column, HiLoad 16/600 Superdex 75 column; flow rate, 1.0 mL/min; buffer, 50 mM potassium phosphate buffer, pH 7.0; temperature, 4 °C, monitoring wavelength 280 (red) and 620 nm (blue).

2.3.4 Spectroscopic and electrochemical characterization of azurin dimer

The oxidized azurin dimer was purified from the solution obtained by the treatment of Cu(II)-azurin with an addition of 140 mM 2-ME at pH 4.0, lyophilization, and dissolution with buffer at pH 7.0. The azurin dimer did not dissociate to monomers up to 60 °C, whereas it dissociated to monomers at 70 °C (Figure 2.12). The high stability of the dimer may correspond to the high stability of the monomer, since the denaturing temperature of the monomer was about 85 °C (Figure 2.12).

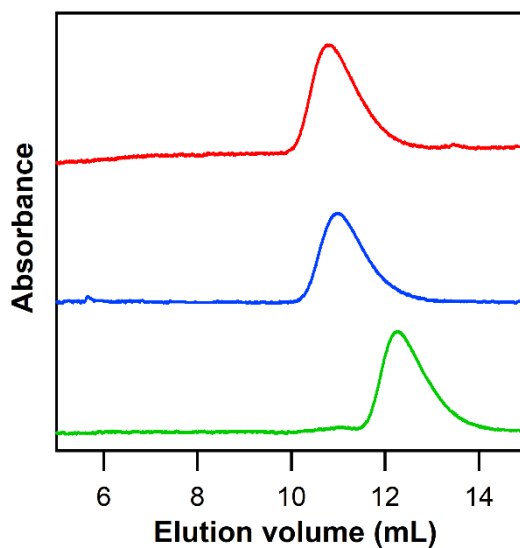


Figure 2.12 SEC chromatograms of the solution obtained before (red) and after incubation of the Cu(II)-azurin dimer solution in potassium phosphate buffer, pH 7.0, at 60 °C (blue) and 70 °C (green) for 1 h. Measurement conditions: column, Superdex 75 10/300 GL; buffer: 50 mM potassium phosphate buffer, pH 7.0; monitoring wavelength: 280 nm.

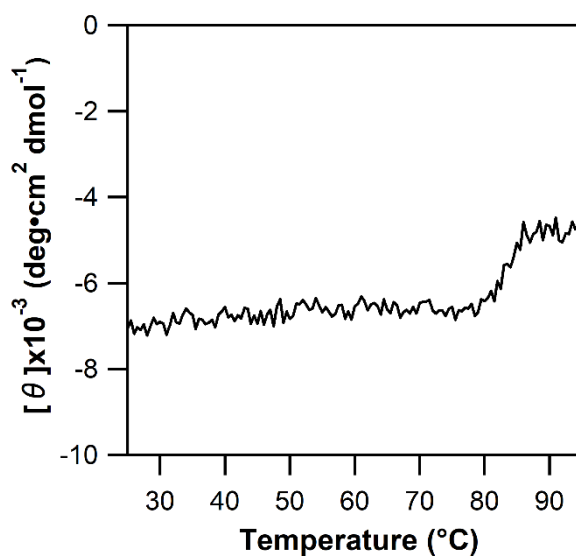


Figure 2.13 CD ellipticity at 222 nm of the azurin monomer at 25–95 °C. Measurement conditions: azurin monomer, 5.0 μM (copper unit); buffer, 50 mM potassium phosphate buffer, pH 7.0; monitoring wavelength 222 nm; scan rate, 1 °C/min.

The wavelength of the maximum absorbance in the visible region of the Cu(II)-azurin dimer was 618 nm, which slightly blue-shifted from that of the monomer at 622 nm. The molar extinction coefficients were obtained as 10,800 and 4,900 $\text{M}^{-1}\text{cm}^{-1}$ at 280 and 622 nm, respectively, for the azurin monomer, and 11,300 and 5,000 $\text{M}^{-1}\text{cm}^{-1}$ (copper unit) at 280 and 618 nm, respectively, for the dimer by inductively coupled plasma mass spectrometry (Fig. 2A). The ratio of the absorbance at 280 nm to that at ~ 620 nm ($\text{Abs}_{280}/\text{Abs}_{618}$) for the Cu(II)-azurin dimer was 2.24, whereas the $\text{Abs}_{280}/\text{Abs}_{622}$ value for the monomer was 2.22. The ratio of the absorption at 460 nm to that at ~ 620 nm for the azurin dimer was 0.113, whereas that for the azurin monomer was 0.067 (Figure 2.14).

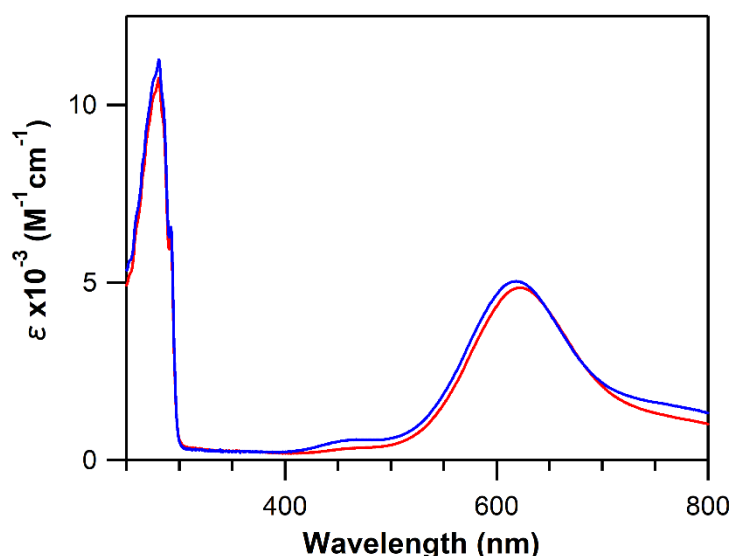


Figure 2.14 Optical absorption spectra of Cu(II)-azurin monomer (red) and dimer (blue): Measurement conditions: azurin (75 μM , copper unit) in 50 mM potassium phosphate buffer, pH 7.0.

The g_{\parallel} and g_{\perp} values obtained from the electron paramagnetic resonance (EPR) spectra (Figure 2.15) were similar between the Cu(II)-azurin monomer and dimer (Table 2.1). However, the A_{\parallel} value of the dimer was 5.845 mT, which was slightly smaller than

that of the monomer (5.950 mT). From these results, a slightly more rhombic character for the active site structure of the dimer is suggested.

Table 2.1. EPR parameters of Cu(II)-azurin monomer and dimer.

	g_{\parallel}	g_{\perp}	A_{\parallel} (mT)
monomer	2.257	2.056	5.950
dimer	2.254	2.057	5.845

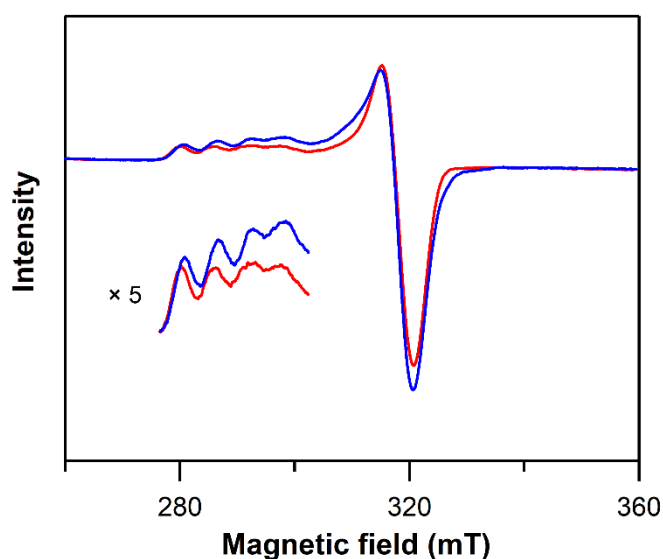


Figure 2.15 EPR spectra of Cu(II)-azurin monomer (red) and dimer (blue). Measurement conditions: azurin (1.0 mM, copper unit) in 100 mM MES buffer, pH 6.5.

According to the circular dichroism (CD) spectra of the Cu(II)-azurin monomer and dimer (Figure 2.16), the β -sheet-related negative Cotton effect around 220 nm was similar between the spectra of the monomer and dimer, indicating similar β -strand structures for the dimer to those of the monomer. However, the intensities of the Cotton effect around 195 nm in the CD spectrum increased slightly by the dimerization, indicating slight changes in the secondary structures between the monomer and dimer.

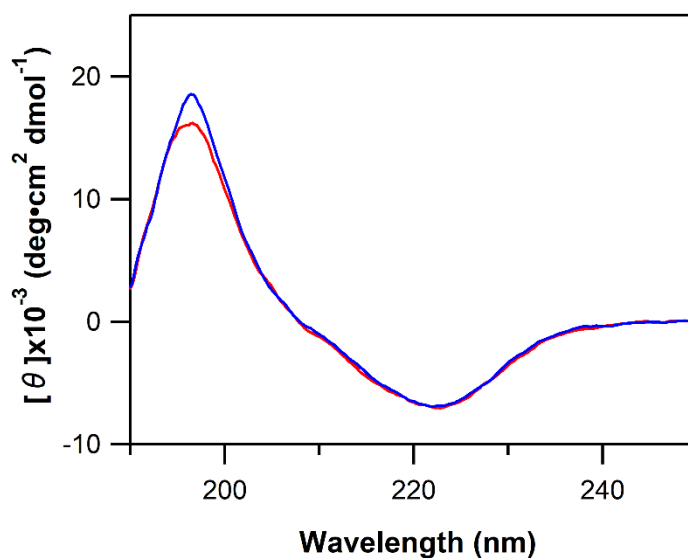


Figure 2.16 CD spectra of Cu(II)-azurin monomer (red) and dimer (blue). Measurement conditions: azurin (5.0 μM , copper unit) in 50 mM potassium phosphate buffer, pH 7.0.

The redox potentials of the azurin monomer and dimer were measured by cyclic voltammetry to investigate the effect of domain swapping on the function. The redox potentials of the azurin monomer and dimer were obtained as 292 ± 5 and 342 ± 5 mV vs NHE, respectively, at pH 6.5 (Figure 2.17), where the redox potential of the monomer was similar to the reported value (305 ± 10 mV) [13]. The redox potential of the dimer was 50 mV higher than that of the monomer, suggesting a weaker Cu coordination structure in the dimer compared to that in the monomer.

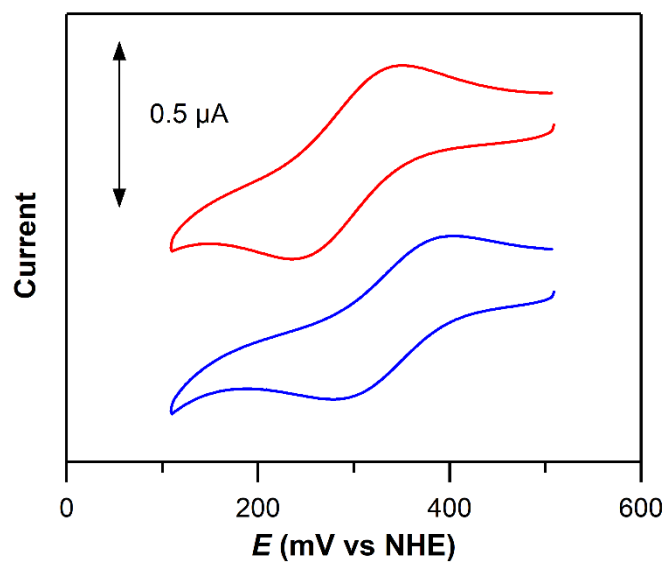


Figure 2.17 Cyclic voltammograms of Cu(II)-azurin monomer (red) and dimer (blue). Measurement conditions: scan rate was 10 mV s^{-1} ; azurin ($200 \text{ } \mu\text{M}$, copper unit) in 100 mM MES buffer, pH 6.5.

2.4 Discussion

The absorption spectra, as well as the EPR parameters, of the monomer and dimer differed slightly (Figure 2.14 and 2.15). Although the EPR spectra of the Cu(II)-azurin monomer and dimer exhibited an axial-type $g_{\parallel} > g_{\perp} > 2$ property, the A_{\parallel} value decreased slightly by the dimerization (Figure 2.15 and Table 1), indicating that the dimer exhibits a slightly more rhombic character than the monomer. Additionally, the intensity of the absorption band at 460 nm to that at ~620 nm was 0.067 and 0.113 for the monomer and dimer, respectively (Figure 2.14), supporting the hypothesis that the rhombic property slightly increases for the dimer compared to the monomer, since the rhombic coordination shows a larger absorption at 460 nm relative to that at ~620 nm [14]. The observation of a rhombic and an axial component in the EPR spectra of pseudoazurins has been interpreted in terms of the presence of two conformations for the copper site [15–17].

The redox potential of the Cu(II)-azurin dimer decreased ~50 mV from that of the monomer (Figure 2.17). The elongation of the copper coordination bonds compared to those in the monomer may contribute to the easier electron acceptor property and higher redox potential for the dimer.

2.5 Conclusion

Cu(I)- and DTT-reduced azurin from *Alcaligenes xylosoxidans* oligomerized by the procedure of addition of 5% v/v (%) TFE at pH 5.0, subsequent lyophilization, and dissolution of the residual at pH 7.0, whereas Cu(II)-azurin oligomerized only slightly by the same procedure, indicating that the reduction of the copper enhances the oligomerization by the procedure. I found that Cu(II)-azurin oligomerizes by the process of an addition of 2-ME at pH 4.0, lyophilization, and dissolution in phosphate buffer at pH 7.0. Although the purified azurin dimer dissociated to monomers by heating at 70 °C for 1 h, it did not dissociate to monomers by heating at 60 °C, indicating that the dimer is relatively stable. The wavelength of the maximum absorbance in the visible region of the azurin dimer was 618 nm, which was slightly blue-shifted from that of the azurin monomer at 622 nm. The ratio of the optical absorbance at 460 nm to that at about 600 nm for the azurin dimer ($A_{460}/A_{618} = 0.113$) was higher than that of the monomer ($A_{460}/A_{622} = 0.067$) and the A_{\parallel} value of the dimer (5.85 mT) in the EPR spectra was slightly lower than that of the monomer (5.95 mT), indicating that the dimer has a little more rhombic Cu coordination character. The redox potential of the azurin dimer was 342 ± 5 mV vs. NHE, which was 50 mV higher than that of the monomer.

References

- [1] Miyamoto, T., Kuribayashi, M., Nagao, S., Shomura, Y., et al., Domain-swapped cytochrome *cb*₅₆₂ dimer and its nanocage encapsulating a Zn-SO₄ cluster in the internal cavity. *Chem. Sci.* 2015, 6, 7336–7342.
- [2] Yamanaka, M., Hoshizumi, M., Nagao, S., Nakayama, R., et al., Formation and carbon monoxide-dependent dissociation of *Allochromatium vinosum* cytochrome *c'* oligomers using domain-swapped dimers. *Protein Sci.* 2017, 26, 464–474.
- [3] Hirota, S., Oligomerization of cytochrome *c*, myoglobin, and related heme proteins by 3D domain swapping. *J. Inorg. Biochem.* 2019, 194, 170–179.
- [4] Nagao, S., Osuka, H., Yamada, T., Uni, T., et al., Structural and oxygen binding properties of dimeric horse myoglobin. *Dalton Trans.* 2012, 41, 11378–11385.
- [5] Hirota, S., Hattori, Y., Nagao, S., Taketa, M., et al., Cytochrome *c* polymerization by successive domain swapping at the C-terminal helix. *Proc. Natl. Acad. Sci. U. S. A.* 2010, 107, 12854–12859.
- [6] Parui, P.P., Deshpande, M.S., Nagao, S., Kamikubo, H., et al., Formation of oligomeric cytochrome *c* during folding by intermolecular hydrophobic interaction between N- and C-terminal α -helices. *Biochemistry* 2013, 52, 8732–8744.
- [7] Deshpande, M.S., Parui, P.P., Kamikubo, H., Yamanaka, M., et al., Formation of domain-swapped oligomer of cytochrome *c* from its molten globule state oligomer. *Biochemistry* 2014, 53, 4696–4703.
- [8] Rosenberger, N., Studer, A., Takatani, N., Nakajima, H., et al., Azurin-poly(*N*-isopropylacrylamide) conjugates by site-directed mutagenesis and their

- thermosensitive behavior in electron-transfer processes. *Angew. Chem. Int. Ed. Engl.* 2009, 48, 1946–1949.
- [9] Fuentes, L., Oyola, J., Fernández, M., Quiñones, E., Conformational changes in azurin from *Pseudomonas aeruginosa* induced through chemical and physical protocols. *Biophys. J.* 2004, 87, 1873–1880.
- [10] Battistuzzi, G., Borsari, M., Sola, M., Francia, F., Redox thermodynamics of the native and alkaline forms of eukaryotic and bacterial class I cytochromes *c*. *Biochemistry* 1997, 36, 16247–16258.
- [11] Yamaguchi, K., Deligeer, Nakamura, N., Shidara, S., et al., Isolation and characterization of two distinct azurins from *Alcaligenes xylosoxidans* subsp. *xylosoxidans* NCIB11015 or GIFU1051. *Chem. Lett.* 1995, 24, 353–354.
- [12] Leckner, J., Wittung, P., Bonander, N., Karlsson, B.G., et al., The effect of redox state on the folding free energy of azurin. *J. Biol. Inorg. Chem.* 1997, 2, 368–371.
- [13] Dodd, F.E., Hasnain, S.S., Hunter, W.N., Abraham, Z.H.L., et al., Evidence for two distinct azurins in *Alcaligenes xylosoxidans* (NCIMB 11015): Potential electron donors to nitrite reductase. *Biochemistry* 1995, 34, 10180–10186.
- [14] Lu, Y., LaCroix, L.B., Lowery, M.D., Solomon, E.I., et al., Construction of a “blue” copper site at the native zinc site of yeast copper-zinc superoxide dismutase. *J. Am. Chem. Soc.* 1993, 115, 5907–5918.
- [15] Comba, P., Müller, V., Remenyi, R., Interpretation of the temperature-dependent color of blue copper protein mutants. *J. Inorg. Biochem.* 2004, 98, 896–902.

- [16] Abdelhamid, R.F., Obara, Y., Uchida, Y., Kohzuma, T., et al., π - π interaction between aromatic ring and copper-coordinated His81 imidazole regulates the blue copper active-site structure. *J. Biol. Inorg. Chem.* 2007, 12, 165–173.
- [17] Gast, P., Broeren, F.G.J., Sottini, S., Aoki, R., et al., The type 1 copper site of pseudoazurin: axial and rhombic. *J. Inorg. Biochem.* 2014, 137, 57–63.

Chapter 3

X-ray crystal structure of azurin dimer

3.1 Introduction

A detailed three-dimensional structure is necessary to understand the properties of the azurin dimer. The most favored technique for structure determination of proteins and biological macromolecules is X-ray crystallography. Obtaining a three dimensional molecular structure from a crystal is the aim of *x*-ray crystallography [1]. The growth of protein crystals of sufficient quality for structure determination is the minimum requirement in most protein crystallographic works. The principle of protein crystallization is to prepare a protein solution with high concentration and induce it to come out from the solution; precipitation will occur if this happens too fast, but crystals will grow under correct conditions [2–4]. Many projects fail because of the inability to crystallize the protein. To obtain a protein crystal, crystallization conditions must be considered [5, 6]: choice and concentration of precipitant, buffer, protein concentration, temperature, crystallization technique, and possible inclusion of additives. Initial experiments will be based on a trial and error procedure, which aims to cover a wide range conditions as possible. Commercially available “crystal screen” packages (usually consists of 50 solutions varying widely in precipitant, buffer, pH, and salt) known as a sparse matrix are often used at this stage [7]. The techniques of sitting drop vapor diffusion, hanging drop vapor diffusion, and possibly dialysis can be set up [8] at various temperatures. In this way, many of the variables can be covered easily, and one or more conditions might even yield crystals of sufficient quality to proceed to the next step.

As discussed in Chapter 2, the dimer dissociated to monomers by heating, and the properties of the monomer and dimer were similar. Although these properties do not contradict that the dimer was formed by domain swapping, domain swapping can only be

proven by the X-ray crystallographic structure at the moment. In this chapter, the X-ray crystal structure of the azurin dimer is revealed, showing that the dimer is formed by domain swapping.

3.2 Materials and methods

3.2.1 X-ray crystallographic analysis

Crystallization of the azurin dimer was performed at 293 K using the sitting drop vapor diffusion method with NeXtal Tubes PEGs Suite (QIAGEN). The protein concentration was adjusted to 1.25 mM (dimer unit) in 10 mM Tris-HCl buffer, pH 8.0. The droplets prepared by mixing 1 μ L of the protein solution with 1 μ L reservoir solution were equilibrated. The best reservoir solution was found to be 20% polyethylene glycol (PEG) 3000 and 100 mM MES buffer, pH 6.5. A crystal was obtained in the protein solution after incubation at 20 °C for 14 days.

The diffraction data were collected at the BL26B1 beamline of SPring-8, Japan. The crystal was mounted on a cryo-loop without an additional cryoprotectant, and flash-frozen at 100 K in a nitrogen cryosystem. The detector was EIGER X 4M (Dectris). The crystal-to-detector distance was 150 mm, and the wavelength was 1.0000 Å. The oscillation angle was 0.1°, and the exposure time was 0.5 seconds per frame. The total number of frames was 1800. The diffraction data were processed using the program XDS [9]. The preliminary structure was obtained by the molecular replacement method (MOLREP [10]) using the atomic coordinates of the monomer structure of azurin-I (PDB ID: 1RKR) as a starting model. The structure refinement was performed using the program REFMAC [11]. The molecular model was manually corrected, and water molecules were picked up in the electron density map using the program COOT [12]. The data collection and refinement statistics are summarized in Table 3.1. The angle ϕ between the N(His)-Cu-N(His) plane and the S(Cys)-Cu-S(Met) plane was calculated using the program Visual Molecular Dynamic.

Table 3.1 Statistics of data collection and structure refinement of the azurin dimer (PDB ID: 6L1V).

Data collection	
X-ray source	SPring-8 (BL26B1)
Wavelength (Å)	1.0000
Space group	C222 ₁
Unit cell parameters	
<i>a</i> , <i>b</i> , <i>c</i> (Å)	107.45, 167.81, 116.99
α , β , γ (°)	90.0, 90.0, 90.0
Resolution (Å)	49.17–2.25 (2.32–2.25)
Number of unique reflections	50385 (4598)
R_{merge}^a	0.079 (1.145)
Completeness (%)	99.9 (100.0)
$\langle I/\sigma(I) \rangle$	12.3 (1.6)
CC _{1/2}	(0.739)
Redundancy	6.8 (7.2)
Refinement	
Resolution (Å)	49.17–2.25 (2.31–2.25)
Number of reflections	47826 (2534)
R_{work}^b	0.20277 (0.327)
R_{free}^b	0.23021 (0.323)
Completeness (%)	99.9 (100.0)
Number of atoms in an asymmetric unit	
Protein	3916
Water	269
Cu	4
Average <i>B</i> factors (Å ²)	
Protein	49.6
Water	49.6
Cu	42.4
Ramachandran plot (%)	
Favored	99.0
Allowed	1.0
Outlier	0

Statistics for the highest-resolution shell are given in parentheses.

$$^a R_{\text{merge}} = \frac{\sum_{\text{hkl}} |I - \langle I \rangle|}{(\sum_{\text{hkl}} |I|)^{-1}}$$

$^b R_{\text{work}} = \frac{\sum_{\text{hkl}} ||F_{\text{obs}}| - k|F_{\text{calc}}||}{(\sum_{\text{hkl}} |F_{\text{obs}}|)^{-1}}$, *k*: scaling factor. R_{free} was computed identically, except where all reflections belong to a test set of 5 % of randomly selected data.

3.3 Results

3.3.1 Protein structure

The blue crystals obtained after 14 days were analysed by X-ray crystallography (Figure 3.1). To elucidate the detailed structure of the azurin dimer, I solved the X-ray crystal structure (PDB ID: 6L1V) at 2.25 Å resolution. The structure contained two asymmetric dimers in the unit cell, where dimer A consisted of protomers 1 and 4, and dimer B consisted of protomers 2 and 3 (Figure 3.2 A). The structure of the azurin dimer exhibited an N-terminal domain-swapped structure, and the N-terminal region containing three β -strands (β -strands 1, 2, and 3) was exchanged three-dimensionally between protomers. Five salt bridges (Lys18_A(N)–Glu19_B(O ϵ), Glu19_A(N)–Glu19_B(O ϵ), Glu19_A(O ϵ)–Glu19_B(N), Glu19_A(O ϵ)–Lys18_B(N), and Lys126_A(N ζ)–Asp16_B(O)) were formed between protomer 1 in dimer A and protomer 2 in dimer B in the unit cell, whereas protomers 3 and 4 did not form salt bridges with the protomers of other dimers (Figure 3.2 B). The hinge loop was constructed with four amino acids: Gly37, Lys38, Leu39, and Ala40. In the dimer structure, β -strand 2 and β -strand 3 in the N-terminal region of a protomer interacted with β -strand 8 and β -strand 6, respectively, in the C-terminal region of the other protomer. The hydrogen bonds between the protomers in the dimer were similar to those observed intramolecularly in the monomer. However, new hydrogen bonds were formed between protomer 1 and protomer 4 (Asp98_{prot1}(O δ)–Gln28_{prot4}(N ϵ) and Lys126_{prot1}(N ζ)–Glu19_{prot4}(O ϵ)) in dimer A (Figure 3.3) and between protomer 2 and protomer 4 (Asp98_{prot2}(O δ)–Gln28_{prot3}(N ϵ) and Lys126_{prot2}(N ζ)–Glu19_{prot3}(O ϵ)) in dimer B.

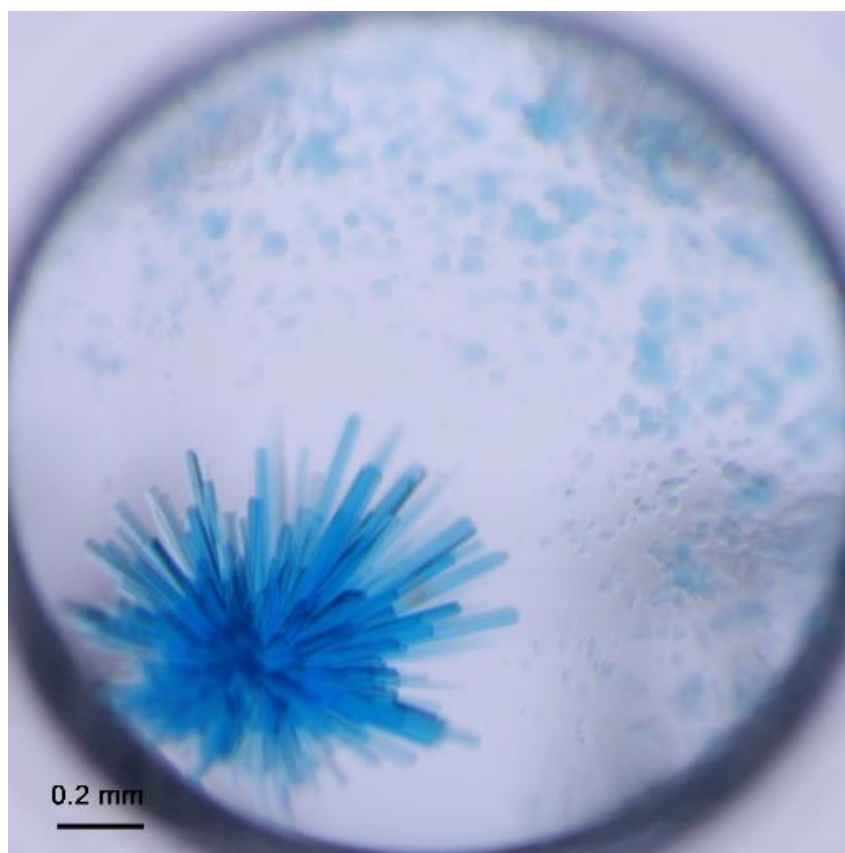


Figure 3.1 Blue crystals of azurin dimers after incubation of the azurin solution at 20 °C for 14 days. The reservoir solution was 100 mM MES buffer, pH 6.5, containing 20% polyethylene glycol (PEG) 3000.

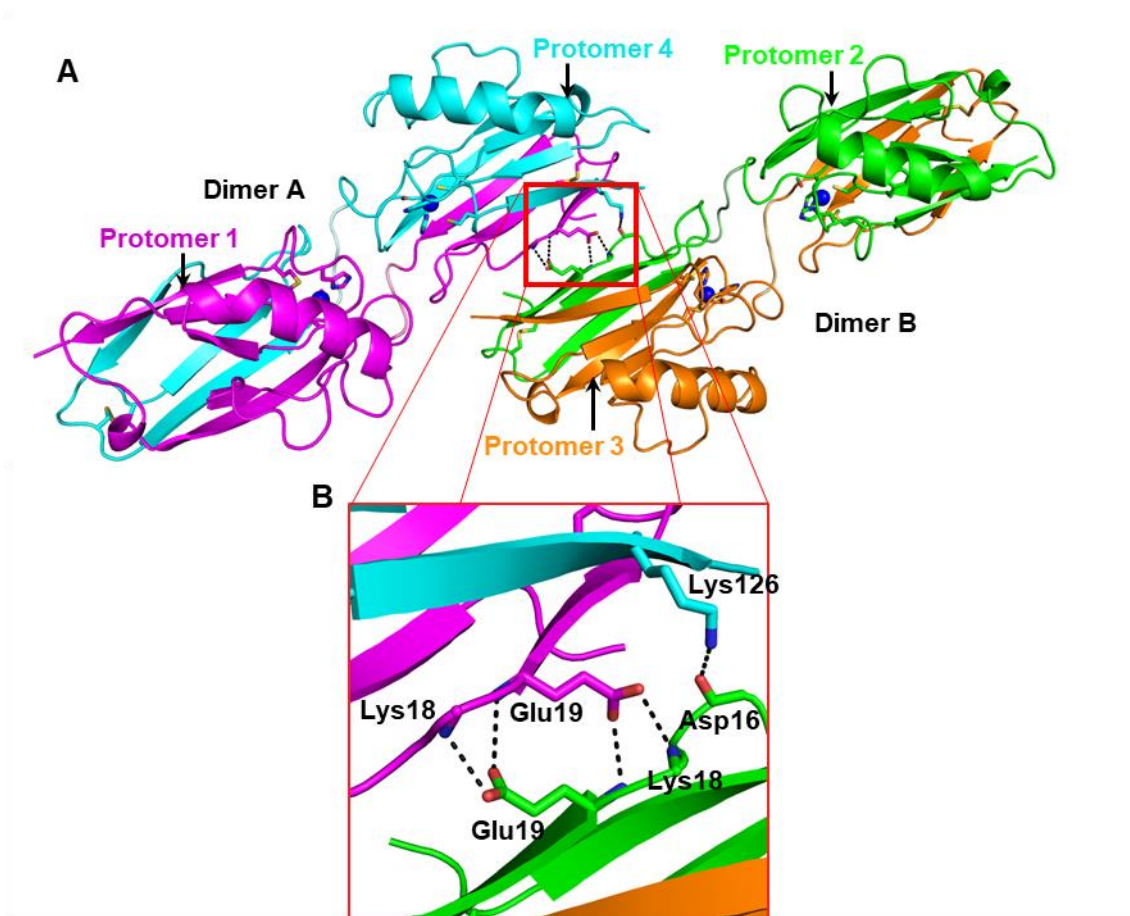


Figure 3.2 Structure of azurin dimers in the unit cell (PDB ID: 6L1V). (A) Protomer 1 (magenta) domain swapped with protomer 4 (cyan) in Dimer A, whereas protomer 2 (green) domain swapped with protomer 3 (orange) in Dimer B. The coppers are shown as sphere models. The main chain of Gly45 and the side chains of Cys3, Cys 26, His46, His117, Cys112, Met121, and Gly45 are shown as stick models. (B) Hydrogen bonds between Dimer A and Dimer B. The hydrogen bonds are depicted in black broken lines. The Gly37–Ala40 residues (hinge loop) are depicted in pale colors. The side chains of Asp16, Lys18, Glu19, Lys126 and main chain carbonyl of Asp16 are shown as stick models. The nitrogen atoms of the main chains of Lys18 and Glu19 and the side chains of His46, His117, and Lys126 are depicted in blue, the oxygen atoms of the main chains of Asp16 and Gly45 and side chains of Glu19 are depicted in red, and the sulfur atoms of Cys3, Cys26, Cys112, and Met121 are depicted in yellow.

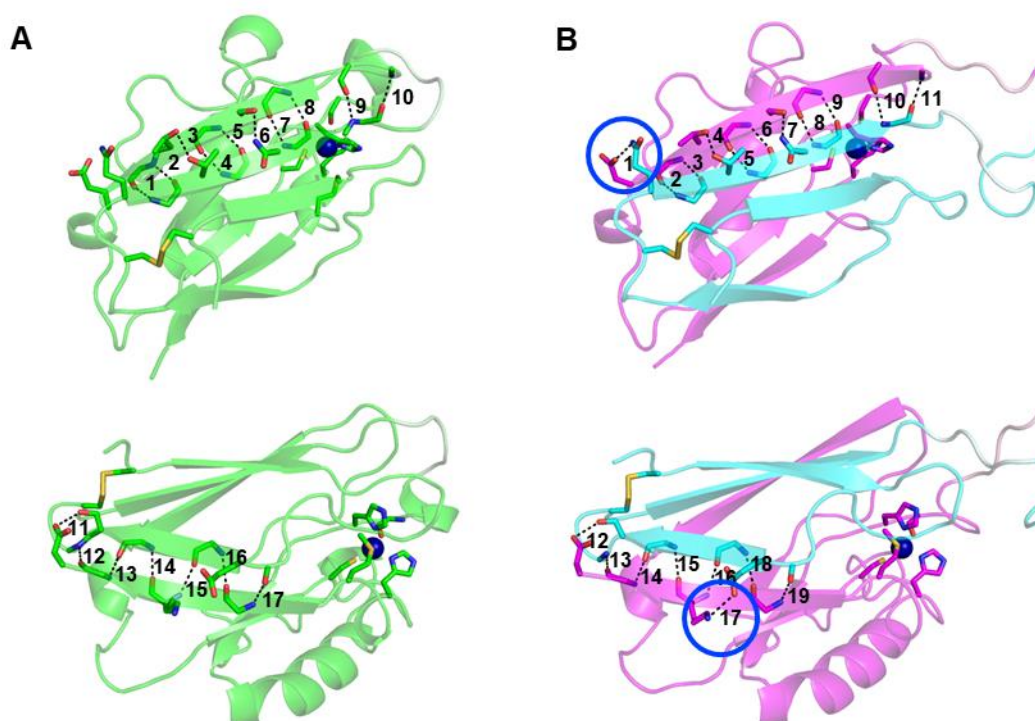


Figure 3.3 Hydrogen bonds between (A) β -strand 2 and β -strand 8 and (B) β -strand 3 and β -strand 6: (A) monomer (green) and (B) dimer A (magenta, protomer 1; cyan, protomer 4). Hydrogen bonds are depicted in black broken lines. The numbers (1–19) denote the hydrogen bonds: monomer, 1: Phe97(O)–Phe29(N), 2: Phe97(N)–Phe29(O), 3: Thr96(O γ)–Thr30(O γ), 4: Val95(O)–Val31(N), 5: Val95(N)–Val31(O), 6: Ser94(O γ)–Asn32(N δ), 7: Asp93(O)–Leu33(N), 8: Asp93(N)–Leu33(O), 9: Glu91(O)–His35(N), 10: Gly90(N)–His35(O), 11: Asp129(O δ)–Ser23(O γ), 12: Val128(O)–Lys24(N), 13: Val128(N)–Val22(O), 14: Lys126(O)–Val22(N), 15: Lys126(N)–Ile20(O), 16: Val124(O)–Ile20(N), 17: Val124(N)–Lys18(O); dimer A, 1: Asp98(O δ)–Gln28(N ϵ) 2: Phe97(O)–Phe29(N), 3: Phe97(N)–Phe29(O), 4: Thr96(O γ)–Thr30(O γ), 5: Val95(O)–Val31(N), 6: Val95(N)–Val31(O), 7: Ser94(O γ)–Asn32(N δ), 8: Asp93(O)–Leu33(N), 9: Asp93(N)–Leu33(O), 10: Glu91(O)–His35(N), 11: Gly90(N)–His35(O), 12: Asp129(O δ)–Ser23(O γ), 13: Val128(O)–Lys24(N), 14: Val128(N)–Val22(O), 15: Lys126(O)–Val22(N), 16: Lys126(N)–Ile20(O), 17: Lys126(N ζ)–Glu19(O ϵ), 18: Val124(O)–Ile20(N), 19: Val124(N)–Lys18(O). The coppers are shown as sphere models. The main chains of

Lys18, Ile 20, Val22, Phe29, Val31, Lys33, His35, Gly45, Gly90, Glu91, Asp93, Val95, Phe97, Val124, Lys126 and Val128, and the side chains of Cys3, Ser23, Cys26, Thr30, Asn32, His46, Ser94, Thr96, His117, Cys112, Met121, and Asp129 are shown as stick models. The Gly37–Ala40 residues (hinge loop) are depicted in pale colors. The nitrogen, oxygen, and sulfur atoms of the amino acids involved in the hydrogen and disulfide bonds are depicted in blue, red, and yellow, respectively.

I calculated the root-mean-square deviation (rmsd) for the C α atoms between the structures of the monomer (PDB ID:1RKR) and dimer. Residues in the N-terminal region (Ala1–Pro36) before the hinge loop (Gly37–Ala40) in a protomer and residues in the C-terminal region (Lys41–Asp129) after the hinge loop in the other protomer in the dimer were compared with the corresponding structural region of the monomer (Figure 3.4 D); the rmsd values were less than 0.90 Å (Table 3.2). These results show that the structures in the monomer and protomers of the dimer are similar. The disulfide bond between Cys3 with Cys26 of the same protomer was also detected in the dimer as in the monomer, and may stabilize the dimer.

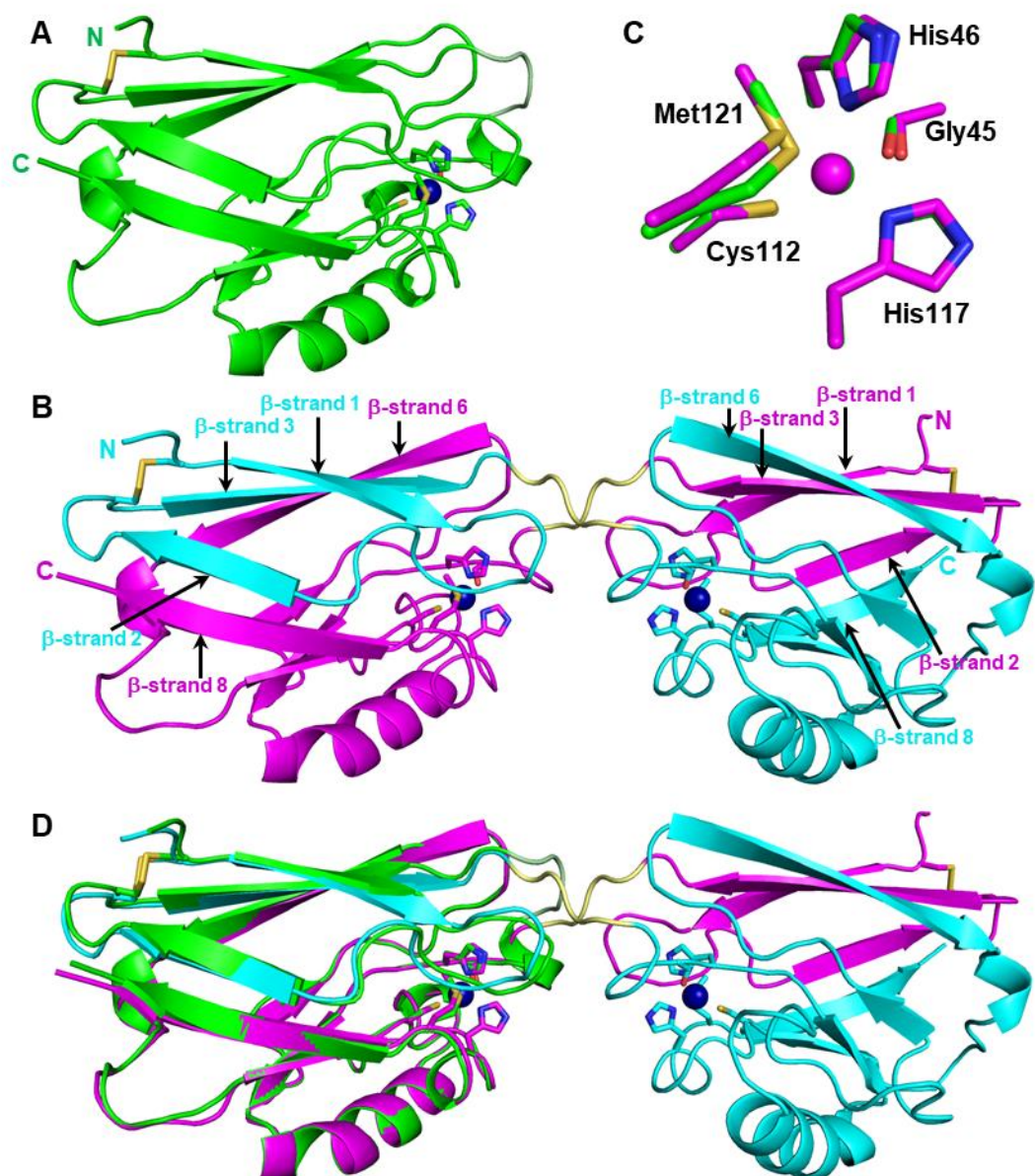


Figure 3.4 Crystal structures of azurin monomer and dimer. (A) Structure of azurin monomer (PDB ID: 1RKR). (B) Structure of azurin dimer A (PDB ID: 6L1V). The two protomers of the dimer are depicted in magenta (protomer 1) and cyan (protomer 4), respectively. (C) Superimposed structures of the copper active sites of the monomer (green) and protomer 1 of dimer A (magenta). (D) Superimposed structures of the azurin monomer and dimer: monomer (PDB ID: 1RKR; green) and dimer (PDB ID: 6L1V; magenta and cyan). The coppers are shown as sphere models. The main chain of Gly45 and the side chains of Cys3, Cys26, His46, His117, Cys112, Met121, and Gly45 are

shown as stick models. The N- and C-termini are labelled as N and C, respectively. The Gly37–Ala40 residues (hinge loop) are depicted in pale colors. The disulfide bonds between Cys3 and Cys26 are depicted in yellow. The nitrogen atoms of the side chains of His46 and His117 are depicted in blue, and the sulfur atoms of Cys3, Cys26, Cys112, and Met121 are depicted in yellow.

Table 3.2 Root-mean-square deviation (RMSD) values for the C α atoms between the structures of the azurin monomer (PDB ID: 1RKR) and domain-swapped dimer (PDB ID: 6LIV).

Unit	RMSD (Å)			
	monomer 1	monomer 2	monomer 3	monomer 4
residues 1-36 of protomer 1 and residues 41-129 of protomer 4	0.79	0.81	0.81	0.79
residues 1-36 of protomer 2 and residues 41-129 of protomer 3	0.86	0.89	0.88	0.87
residues 1-36 of protomer 3 and residues 41-129 of protomer 2	0.81	0.83	0.84	0.81
residues 1-36 of protomer 4 and residues 41-129 of protomer 1	0.81	0.83	0.84	0.81

3.3.2 Active site structure

Similar to the active site structure of the azurin monomer, the N atoms of the imidazoles of His46 and His117 and the S atom of Cys112 coordinated to the Cu atom in a distorted trigonal plane in the azurin dimer, and the S atom of Met121 and the carbonyl O atom of Gly45 coordinated to the Cu atom axially (Figure 3.4 C). Although the Cu–N(His46) and Cu–S(Cys112) distances in the dimer were similar to the corresponding

distances in the monomer, most of the copper coordination distances increased in the dimer compared to those in the monomer (Table 3.3). Especially, the Cu–O(Gly45) distance in the dimer was 0.4–0.8 Å longer than that in the monomer. The hydrogen bond between His46 and Asn10 was observed in the monomer structure, but not in the dimer structure (Figure 3.5) The Asn10–His46 distances are shown in Table 3.4.

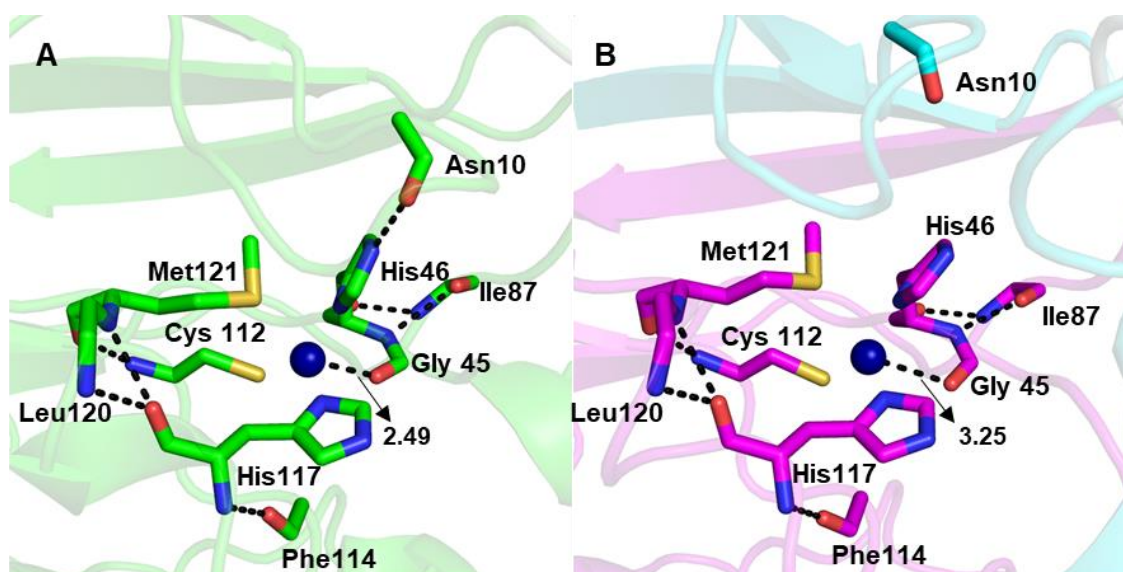


Figure 3.5 Structures of azurin monomer and dimer around the copper site: (A) monomer (PDB ID: 1RKR; green) and (B) dimer A (PDB ID: 6L1V; magenta and cyan). The copper are shown as sphere models. The two protomers of the dimer are depicted in magenta and cyan, respectively. Main chains of Asn10, Gly45, His46, Ile87, Cys112, Phe114, His117, Leu120, Met121 and side chains of His46, Cys112, His117, Met121 are shown as stick models. Hydrogen bonds are depicted in black broken lines. The Gly37–Ala40 residues (hinge loops) are depicted in pale colors. The nitrogen atoms of the main chains of His46, Ile87, Cys112, His117, Leu120, and Met121 and side chains of His46 and His117 are depicted in blue, the oxygen atoms of the main chains of Asn10, Gly45, His46, Ile87, Phe114, and His117 are depicted in red, and the sulfur atoms of Cys112 and Met121 are depicted in yellow.

Table 3.3 Copper coordination bond lengths of azurin monomer and dimer.

	Monomer [13]	dimer			
	(Å)	prot1 (Å)	prot2 (Å)	prot3 (Å)	prot4 (Å)
Cu–N(His46)	1.88–2.03	2.00	2.02	1.98	1.99
Cu–N(His117)	1.87–1.99	2.02	2.04	2.08	2.09
Cu–S(Cys112)	2.12–2.24	2.29	2.24	2.23	2.20
Cu–S(Met121)	3.14–3.24	3.30	3.36	3.00	3.05
Cu–O(Gly45)	2.46–2.59	3.00	2.98	3.24	3.25

Table 3.4 Asn10–His46 distances of azurin monomer and dimer.

	Monomer [13]	dimer			
	(Å)	prot1 (Å) (prot1– prot4)	prot2 (Å) (prot2– prot3)	prot3 (Å) (prot3– prot2)	prot4 (Å) (prot4– prot1)
Asn10–His46	2.79–2.84	5.52	5.49	5.84	5.75

3.4 Discussion

The dihedral angle φ between the N(His)-Cu-N(His) plane and the S(Cys)-Cu-S(Met) plane in the azurin dimer was 83.8–86.0°, which value was close to 90°, indicating that the copper site was tetrahedrally distorted, whereas the dihedral angle φ was 73.8–78.7° in the monomer. The rhombic interaction derives from the strong thiolate-Sp π interaction with the copper, which rises the energy of the $d_{x^2-y^2}$ orbital relative to that of the d_{xy} orbital [14–16]. The observation of a rhombic and an axial component in the EPR spectra of pseudoazurins has been interpreted in terms of the presence of two conformations for the copper site [17–19]. The hydrogen bond between Asn10 and His46, which was formed in the monomer, was cleaved in the domain-swapped dimer (Figure 3.6). Owing to the cleavage of this hydrogen bond, the copper site of the domain-swapped azurin dimer may be more flexible than that of the monomer, which may increase the rhombic component in the dimer.

Differences were observed in the bond lengths at the copper site between the protomers of the dimer in the crystal (Table 3.3). Five salt bridges (Lys18_A(N)–Glu19_B(O ϵ), Glu19_A(N)–Glu19_B(O ϵ), Glu19_A(O ϵ)–Glu19_B(N), Glu19_A(O ϵ)–Lys18_B(N), and Lys126_A(N ζ)–Asp16_B(O)) were formed between protomer 1 in dimer A and protomer 2 in dimer B in the unit cell, whereas protomers 3 and 4 did not form salt bridges with the protomers of other dimers (Figure 3.2). These salt bridges may cause structural perturbation at the active site; thus, the active site geometries of protomers 1 and 2 with interprotomer salt bridges were similar, and those of protomers 3 and 4 without these salt bridges were similar. Most of the copper coordination distances

increased in the dimer compared to those of the monomer; especially the axial Cu–O(Gly45) bond length was 0.4–0.8 Å longer for the dimer (Figure 3.5 C and Table 2). Since His46 is located next to Gly45, the cleavage of the hydrogen bond involving His46 may cause perturbation at the copper site and elongation of the Cu–O(Gly45) bond (Figure 3.6). The elongation of the copper coordination bonds compared to those in the monomer may contribute to the easier electron acceptor property and higher redox potential for the dimer (Figure 2.16).

Since the activation enthalpy is large for domain swapping [20–25], domain swapping apparently occurred during the dissolution (refolding) process of azurin in the present study. The N- and C-terminal α -helices interact between each other at the early stage of folding in cyt *c* [26, 27], and domain-swapped oligomers are formed when the α -helices interact intermolecularly [28]. A molecular dynamics simulation study showed that the separation between the monomer folding and domain swapping in the folding pathway of apomyoglobin occurs at the early stage of folding [29]. RNase A also domain swaps during refolding from the urea- or guanidinium ion-denatured state [30]. For azurin unfolding, the β 2– β 8 and β 7– β 8 contacts are ruptured first, followed by rupture of all remaining β -strand pairs (β 1– β 3, β 3– β 6, β 4– β 7 and β 5– β 6) [31, 32]. The domain-swapped dimer of azurin may form by the intermolecular interaction between β -strand 3 of a molecule with β -strand 6 of another molecule at the initial stage of folding during the dissolution process after lyophilization, whereas the intramolecular interaction between these β -strands results in the formation of monomers (Figure 3.7). Concerning copper binding to the apoprotein, there are two pathways for the formation of holoazurin: copper binding before polypeptide folding and copper binding after polypeptide folding [33, 34].

Interestingly, the amount of oligomers of azurin increased by the addition of Cu(II) ions during the dissolution process (Figure 3.7). These results indicate that Cu(II) ions may stabilize the protein region containing the Cu(II) ion and enhance the intermolecular interaction between the swapping region of a molecule with the rest of the protein of another molecule during folding of azurin (Figure 3.7).

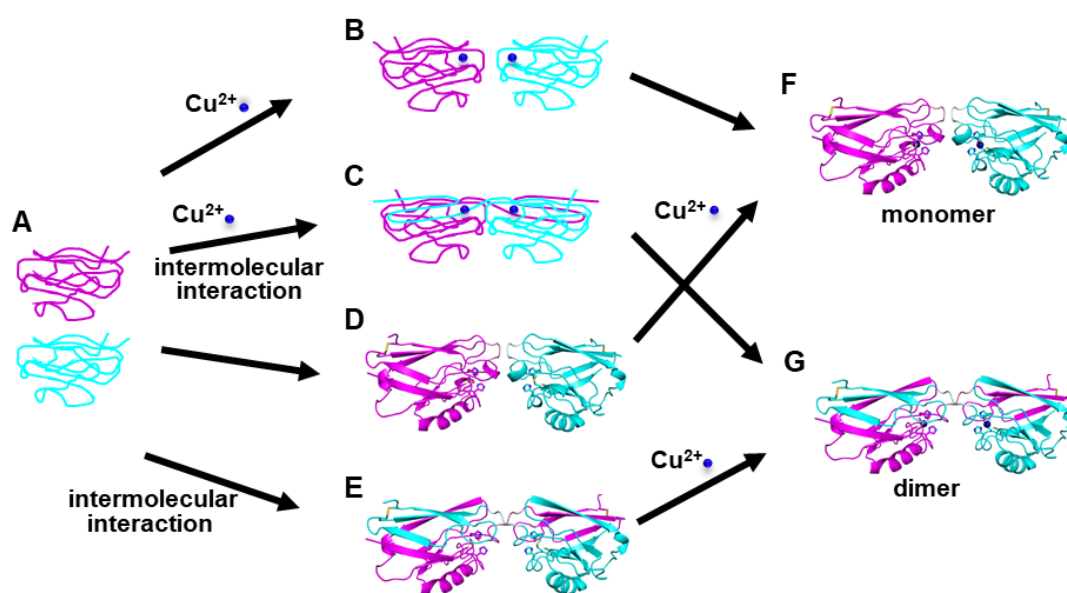


Figure 3.7 Schematic view of the dimerization and copper binding processes during folding of azurin. (A) Unfolded azurin. (B) Unfolded azurin monomer with copper. (C) Unfolded azurin dimer with copper. (D) Folded apoazurin monomer. (E) Folded apoazurin dimer. (F) holoazurin monomers (PDB ID: 1RKR). (G) Domain-swapped holoazurin dimer (PDB ID: 6L1V). In the presence of Cu(II) ions, the folding process from A to C is enhanced, increasing the formation of dimer G.

3.5 Conclusion

The X-ray crystal structure of the azurin dimer was solved at 2.25 Å resolution, where three β-strands (β-strands 1, 2, and 3) in the N-terminal region were exchanged between protomers. Two asymmetric dimers were included in the unit cell, and the dimers interacted between each other by five hydrogen bonds. The hydrogen bonds between the protomers in the dimer were similar to those observed intramolecularly in the monomer, whereas two new hydrogen bonds were formed between protomer 1 and protomer 4 in dimer A. The rmsd value for the C α atoms between the structures of the monomer and dimer were less than 0.90 Å, indicating that the structures in the monomer and protomers of the dimer are similar. The copper coordination structure in the azurin dimer was tetrahedrally distorted, in a similar way to that in the monomer; however, the Cu–O(Gly45) bond length was 0.4–0.8 Å longer for the dimer. The Cu(II) ion may stabilize the protein region containing the Cu(II) ion and enhance the intermolecular interaction between the swapping region of a molecule with the rest of the protein of another molecule during folding of azurin.

References

- [1] Smyth, M.S., Martin, J.H., X ray crystallography. *Mol. Pathol.* 2000, 53, 8–14.
- [2] Gernert, K.M., Smith, R., Carter, D.C., A simple apparatus for controlling nucleation and size in protein crystal growth. *Anal. Biochem.* 1988, 168, 141–147.
- [3] Wilson, L.G., Bray, T.L., Suddath, F.L., Crystallization of proteins by dynamic control of evaporation. *J. Cryst. Growth* 1991, 110, 142–147.
- [4] Luft, J.R., Arakali, S. V., Kirisits, M.J., Kalenik, J., et al., Macromolecular crystallization procedure employing diffusion cells of varying depths as reservoirs to tailor the time course of equilibration in hanging- and sitting-drop vapor-diffusion and microdialysis experiments. *J. Appl. Crystallogr.* 1994, 27, 443–452.
- [5] Carter Jr., C.W., Carter, C.W., Protein crystallization using incomplete factorial experiments. *J. Biol. Chem.* 1979, 254, 12219–12223.
- [6] Carter, C.W., Baldwin, E.T., Frick, L., Statistical design of experiments for protein crystal growth and the use of a precrystallization assay. *J. Cryst. Growth* 1988, 90, 60–73.
- [7] Jancarik, J., Kim, S.H., Sparse matrix sampling. A screening method for crystallization of proteins. *J. Appl. Crystallogr.* 1991, 24, 409–411.
- [8] Krauss, I.R., Merlino, A., Vergara, A., Sica, F., An overview of biological macromolecule crystallization. *Int. J. Mol. Sci.* 2013, 14, 11643–11691.
- [9] Kabsch, W., XDS. *Acta Cryst.* 2010, 66, 125–132.
- [10] Vagin, A., Teplyakov, A., MOLREP: an automated program for molecular replacement. *J. Appl. Cryst.* 1997, 30, 1022–1025.

- [11] Brünger, A.T., Adams, P.D., Clore, G.M., Delano, W.L., et al., Crystallography & NMR system: a new software suite for macromolecular structure determination. *Acta Cryst.* 1998, 54, 905–921.
- [12] Emsley, P., Cowtan, K., Coot: model-building tools for molecular graphics. *Acta Cryst.* 2004, 60, 2126–2132.
- [13] Li, C., Inoue, T., Gotowda, M., Suzuki, S., et al., Structure of azurin I from the denitrifying bacterium *Alcaligenes xylosoxidans* NCIMB 11015 at 2.45 Å resolution. *Acta Cryst.* 1998, 54, 347–354.
- [14] Penfield, K.W., Gewirth, A.A., Solomon, E.I., Electronic Structure and Bonding of the Blue Copper Site in Plastocyanin. *J. Am. Chem. Soc.* 1985, 107, 4519–4529.
- [15] Gewirth, A.A., Solomon, E.I., Electronic Structure of Plastocyanin: Excited State Spectral Features. *J. Am. Chem. Soc.* 1988, 110, 3811–3819.
- [16] Pierloot, K., De Kerpel, J.O.A., Ryde, U., Olsson, M.H.M., et al., Relation between the structure and spectroscopic properties of blue copper proteins. *J. Am. Chem. Soc.* 1998, 120, 13156–13166.
- [17] Comba, P., Müller, V., Remenyi, R., Interpretation of the temperature-dependent color of blue copper protein mutants. *J. Inorg. Biochem.* 2004, 98, 896–902.
- [18] Abdelhamid, R.F., Obara, Y., Uchida, Y., Kohzuma, T., et al., π - π interaction between aromatic ring and copper-coordinated His81 imidazole regulates the blue copper active-site structure. *J. Biol. Inorg. Chem.* 2007, 12, 165–173.
- [19] Gast, P., Broeren, F.G.J., Sottini, S., Aoki, R., et al., The type 1 copper site of pseudoazurin: axial and rhombic. *J. Inorg. Biochem.* 2014, 137, 57–63.

- [20] Jerala, R., Žerovnik, E., Accessing the global minimum conformation of stefin A dimer by annealing under partially denaturing conditions. *J. Mol. Biol.* 1999, 291, 1079–1089.
- [21] Rousseau, F., Schymkowitz, J.W.H., Wilkinson, H.R., Itzhaki, L.S., Three-dimensional domain swapping in p13suc1 occurs in the unfolded state and is controlled by conserved proline residues. *Proc. Natl. Acad. Sci. U. S. A.* 2001, 98, 5596–5601.
- [22] Liu, L., Byeon, I.J.L., Bahar, I., Gronenborn, A.M., Domain swapping proceeds via complete unfolding: A ¹⁹F- and ¹H-NMR study of the cyanovirin-N protein. *J. Am. Chem. Soc.* 2012, 134, 4229–4235.
- [23] Hayashi, Y., Nagao, S., Osuka, H., Komori, H., et al., Domain swapping of the heme and N-terminal α -helix in *Hydrogenobacter thermophilus* cytochrome c552 dimer. *Biochemistry* 2012, 51, 8608–8616.
- [24] Hirota, S., Yamashiro, N., Wang, Z., Nagao, S., Effect of methionine80 heme coordination on domain swapping of cytochrome c. *J. Biol. Inorg. Chem.* 2017, 22, 705–712.
- [25] Hirota, S., Oligomerization of cytochrome c, myoglobin, and related heme proteins by 3D domain swapping. *J. Inorg. Biochem.* 2019, 194, 170–179.
- [26] Roder, H., Elöve, G.A., Englander, S.W., Structural characterization of folding intermediates in cytochrome c by H-exchange labelling and proton NMR. *Nature* 1988, 335, 700–704.

- [27] Hu, W., Kan, Z.-Y., Mayne, L., Englander, S.W., Cytochrome c folds through foldon-dependent native-like intermediates in an ordered pathway. *Proc. Natl. Acad. Sci. U. S. A.* 2016, 113, 3809–3814.
- [28] Parui, P.P., Deshpande, M.S., Nagao, S., Kamikubo, H., et al., Formation of oligomeric cytochrome c during folding by intermolecular hydrophobic interaction between N- and C-terminal α -helices. *Biochemistry* 2013, 52, 8732–8744.
- [29] Ono, K., Ito, M., Hirota, S., Takada, S., Dimer domain swapping versus monomer folding in apo-myoglobin studied by molecular simulations. *Phys. Chem. Chem. Phys.* 2015, 17, 5006–5013.
- [30] López-Alonso, J.P., Bruix, M., Font, J., Ribó, M., et al., NMR spectroscopy reveals that RNase A is chiefly denatured in 40% acetic acid: Implications for oligomer formation by 3D domain swapping. *J. Am. Chem. Soc.* 2010, 132, 1621–1630.
- [31] Beedle, A.E.M., Lezamiz, A., Stirnemann, G., Garcia-Manyes, S., The mechanochemistry of copper reports on the directionality of unfolding in model cupredoxin proteins. *Nat. Commun.* 2015, 6, 7894 (9 pages).
- [32] Yadav, A., Paul, S., Venkatramani, R., Ainavarapu, S.R.K., Differences in the mechanical unfolding pathways of apo- and copper-bound azurins. *Sci. Rep.* 2018, 8, 1989 (13 pages).
- [33] Pozdnyakova, I., Wittung-Stafshede, P., Copper binding before polypeptide folding speeds up formation of active (holo) *Pseudomonas aeruginosa* azurin. *Biochemistry* 2001, 40, 13728–13733.

- [34] Palm-Espling, M.E., Niemiec, M.S., Wittung-Stafshede, P., Role of metal in folding and stability of copper proteins in vitro. *Biochim. Biophys. Acta* 2012, 1823, 1594–1603.

Chapter 4
General conclusion

It has been reported that many proteins can form domain-swapped oligomers by treatment with ethanol or acetic acid. However, domain swapping oligomerization of copper proteins has not been reported. Thus, in this thesis, I investigated the domain swapping oligomerization of a blue copper protein azurin from *Alcaligenes xylosoxidans*.

Cu(II)-azurin-I from *Alcaligenes xylosoxidans* slightly oligomerized by the procedure of an addition of 5% (v/v) TFE at pH 5.0, lyophilization, and dissolution of the residual to buffer at pH 7.0, whereas Cu(I)- and DTT-reduced azurins oligomerized in larger amount by the same procedure, indicating that the reduction of the copper ion enhances the oligomerization by the procedure. I found that Cu(II)-azurin oligomerizes by the process of an addition of 2-ME at pH 4.0, lyophilization, and dissolution in phosphate buffer at pH 7.0. The azurin dimer did not dissociate to monomers by heating at 60 °C for 1 h, indicating that the dimer is relatively stable. Since azurin oligomerized by the procedure using 2-ME, this procedure may be applied to other metalloproteins. An additional peak of an azurin trimer was detected in the SEC chromatogram after treatment with 2-ME. I expect that the azurin trimer will be purified in a further study, allowing its three-dimensional structure to be elucidated.

The wavelength of the maximum absorbance in the visible region of the azurin dimer was 618 nm, which was slightly blue-shifted from that of the azurin monomer at 622 nm. The ratio of the optical absorbance at ~460 nm to that at about ~620 nm increased for the dimer compared to that of the monomer and the EPR A_{\parallel} value of the dimer decreased compare to that of the monomer, indicating that the dimer has a little more rhombic copper coordination character. However, the secondary structures of the Cu(II)-azurin dimer were similar to those of the monomer according to the CD measurements. The redox

potential of the domain-swapped azurin dimer was 50 mV higher than that of the monomer, presumably due to elongation of the Cu–O(Gly45) bond by the domain-swapping induced cleavage of the hydrogen bond involving His46. I hope the electron transfer property of the azurin dimer will be clarified in the future.

The X-ray crystal structure of the azurin dimer was solved at 2.25 Å resolution, where three β -strands (β -strands 1, 2, and 3) in the N-terminal region were exchanged between protomers. The rmsd value for the $C\alpha$ atoms between the structures of the monomer and dimer show that the structures in the monomer and protomers of the dimer are similar. The copper coordination structure in the azurin dimer was tetrahedrally distorted, in a similar way to that in the monomer. The Cu(II) ion may stabilize the protein region containing the Cu(II) ion and enhance the intermolecular interaction between the swapping region of a molecule with the rest of the protein of another molecule during folding of azurin. I have proposed the azurin oligomerization mechanism during folding, but additional experiments are needed to verify the proposal. Since ions affect protein folding, I hope that the effects of ions on azurin oligomerization will be elucidated in the future.

Acknowledgment

First, I would like to express my deepest gratitude to Allah Almighty who gave me the courage, health and energy to accomplish my thesis. The most sincere appreciation is delivered to Professor Shun Hirota, my academic supervisor for his guidance, supervision and encouragement and also for the valuable time he has devoted to all periods of my study in Japan.

I would like to thank the supervisor committee, Professor Kiyomi Kakiuchi, Profesor Hironari Kamikubo and Assistant Professor Masaru Yamanaka for their constructive comments and suggestions. A sincere gratitude is presented to Assistant Professor Masaru Yamanaka for his supports and assistance during my study. I would like to thank Associate Professor Takashi Matsuo, Assistant Professor Satoshi Nagao for providing supports and sharing their experience as well as knowledge.

I am really grateful to the Ministry of Research and Higher Education of Republic of Indonesia, through the Directorate General of Higher Education (DGHE) for the Doctoral Scholarship (BPPLN). I truly appreciate the president of Nara Institute Science and Technology and the Dean of the Graduate School of Materials Science for the financial support through the teaching assistant.

I am so thankful to Dr. Mohan Zhang, Dr. Hisashi Kobayashi, Dr. Takaaki Miyamoto, Dr Akiya Oda, Dr. Hongxu Yang and other members of Supramolecular Science Laboratory, for their support in experiments and valuable friendship. I would like to appreciate Mrs. Masako Tashiro for her kindness help in the daily life. My great gratitude is presented to the NAIST International Student Affair section for helping me, for both the school and life, during my stay in Nara.

Finally, I am so grateful to my family, especially my mother, for their endless support and praying to complete this study. The most important part of my life, my lovely wife Sovi Delianti Annanda, words cannot express how grateful I am for your support, understanding, comprehension and patience during the Doctoral study. And to my sons, Daffi Kevna Fatin and Raskha Abizar Ramadhan, the spirit you gave to me to accomplish this study is greatly appreciated.

List of Publications

1. 3D domain swapping of azurin from *Alcaligenes xylosoxidans*.

Robby Noor Cahyono, Masaru Yamanaka, Satoshi Nagao, Naoki Shibata, Yoshiki Higuchi, and Shun Hirota, submitted.